ERDC/ITL TR-23-3

US Army Corps
of Engineers®
Engineer Research and
Development Center

Navigation Systems Research Program

Repair of Corroded Steel Girders of Hydraulic Steel Structures (HSS) Using Fiber-Reinforced Polymers (FRP)

Felipe J. Acosta and Guillermo A. Riveros

August 2023

Information Technology Laboratory

The US Army Engineer Research and Development Center (ERDC) solves the nation's toughest engineering and environmental challenges. ERDC develops innovative solutions in civil and military engineering, geospatial sciences, water resources, and environmental sciences for the Army, the Department of Defense, civilian agencies, and our nation's public good. Find out more at www.erdc.usace.army.mil.

To search for other technical reports published by ERDC, visit the ERDC online library at https://erdclibrary.on.worldcat.org/discovery.

ERDC/ITL TR-23-3
August 2023

Repair of Corroded Steel Girders of Hydraulic Steel Structures (HSS) Using Fiber-Reinforced Polymers (FRP)

Guillermo A. Riveros

US Army Engineer Research and Development Center (ERDC)
Information Technology Laboratory (ITL)
3909 Halls Ferry Road
Vicksburg, MS 39180-6199

Felipe J. Acosta

University of Puerto Rico, Mayaguez Campus
Department of Civil Engineering and Surveying
PO Box 9000
Mayaguez, PR 00680

Final Technical Report (TR)

Prepared for Engineer Research Development Center
Navigation Systems Research Program
Vicksburg, MS 39180-6199

Under Work Unit 05D8DB, “FRP to strengthen deteriorated HSS,” Funding Account Code U4388303 / AMSCO Code 031391

Abstract

Although steel hydraulic structures have a protective system to prevent corrosion, this type of deterioration will eventually occur due to the constant exposure to harsh environmental conditions. There are several techniques that can be implemented to repair corroded steel structural elements. This report presents a numerical study to evaluate the mechanical behavior of corroded steel girders used in hydraulic steel structures and to evaluate several carbon fiber–reinforced polymers (CFRP) layups to repair them. The girders were modeled as simply supported with four-point loading boundary conditions. The corrosion deterioration was modeled as loss in section as 10%, 25%, and 40%. The effectiveness of the deterioration was established based on the level of stresses at the steel compared with the undamaged condition after it is strengthened with CFRP. It was found that CFRP repair is more practical for reducing the stresses at the steel in the shear dominated zone if deterioration is below 25%. At the tensile dominated zone, CFRP is effective for reducing the stresses for deterioration below 40%.

Contents

Figures and Tables

Figures

Tables

Preface

This research was conducted for the US Army Engineer Research and Development Center (ERDC) Navigation Systems Research Program under Work Unit 05D8DB, "FRP to strengthen deteriorated HSS." The program manager was Morgan Johnston, Coastal and Hydraulics Laboratory, ERDC, Vicksburg, MS.

The work was performed by the Information Technology Laboratory, ERDC. At the time of publication, Dr. Jeffrey L. Hensley was chief, Computational Science and Engineering Division; Dr. Robert M. Wallace was technical director; Dr. Jackie S. Pettway was deputy director; and Dr. David A. Horner was director.

COL Christian Patterson was commander of ERDC, and Dr. David W. Pittman was director.

This page intentionally left blank.

1 Introduction

1.1 Background

Hydraulic steel structures (HSS) such as locks gates, spillway gates, and maintenance closure structures may have fabrication defects and flaws that can be large enough to threaten the structure's integrity. In addition to the fabrication defects and flaws, the nation's HSS is suffering significant deterioration caused by combined effects of several complex phenomena, including corrosion, cracking and fatigue, impact, and overloads (Riveros and Arredondo 2010, 2014). The structural systems are also suffering from the deterioration of the design boundary conditions (Riveros et al. 2022). An example of severe pitting corrosion in a miter gate pintle is shown in Figure 1. Examples of HSS with existing flaws, fatigue cracks, and significant deterioration include existing torch-cut drain hole of a bulkhead, significant corrosion, edge cracks, incomplete joint penetration, center cracks, buried penny-shaped cracks, pitting corrosion, and other defects (Dexter et al. 2007).

Figure 1. Pitting corrosion on a miter gate pintle.

1.2 Corrosion and Section Loss

Steel corrosion is degradation of a material caused by reaction with its environment. All corrosion processes include electrochemical reactions. Galvanic corrosion, pitting corrosion, crevice corrosion, and general corrosion are purely electrochemical. Erosion corrosion and stress corrosion, however, result from the combined action of chemical plus mechanical factors. Corrosion leads to section loss that affects the capacity, safety, and life of the HSS (Sauser and Riveros 2009). Examples of corrosion and section loss are shown in Figure 2.

Figure 2. Examples of corrosion and section loss.

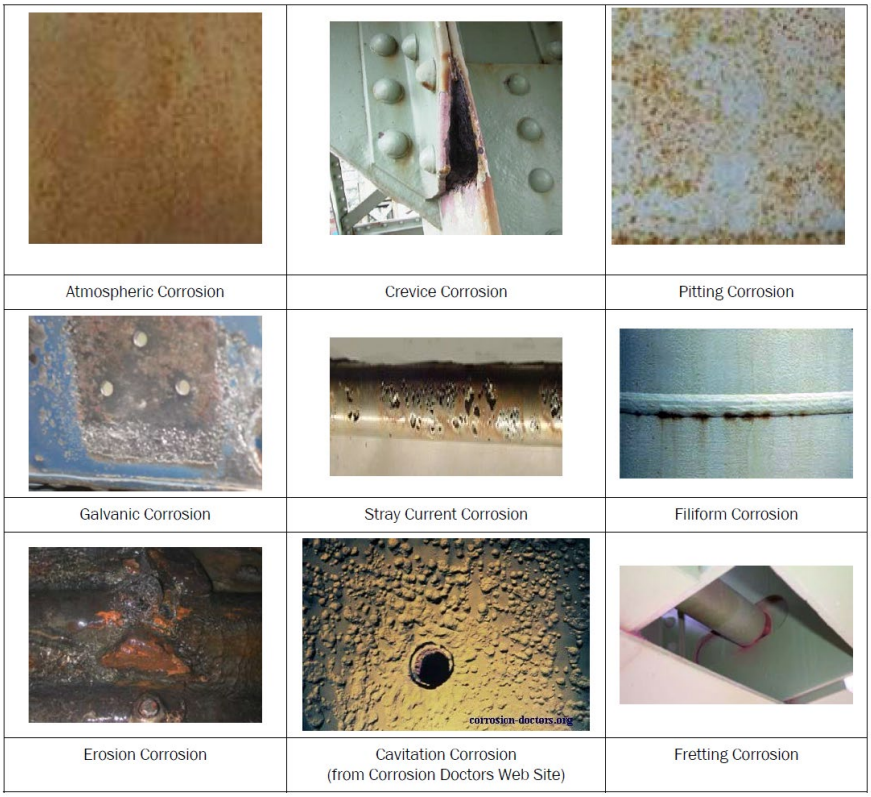

1.3 Repairing Corroded Steel

Different traditional approaches were adapted to repair the structural steel corrosion, including repairing any cracks, applying a protective coating, and welding or bolting steel plates to enhance the corroded steel section (Jayasuriya et al. 2018). However, recently, using fiber-reinforced polymers started to gain attention as an effective and less labor-intensive solution compared with other approaches (Mitra et al. 2020; Sirimanna et al. 2015). Repairing the various steel elements with a different type of fiber-reinforced fabrics has been discussed before in other studies (Mahmoud et al. 2018; Riveros et al. 2018). Different approaches were adapted to understand the effect of utilizing these fabrics on the steel elements' performance, classified into experimental, analytical, and numerical approaches. A discussion of these current approaches is provided here.

Andresen and Echtermeyer (2006) experimentally and analytically investigated the adhesive strength of the carbon laminate attached to a steel plate using a glass fiber–reinforced adhesive. Double cantilever beam and end notched flexure tests were utilized to estimate Mode I and Mode II's energy release rates. The study concluded that the energy release rate of

this system's interface was higher in Mode I than in Mode II. Haghani and Al-Emrani (2012a; 2012b) introduced a new design model for the adhesive joints between fiber-reinforced polymer laminates to steel beams that can be used for strengthening and repair purposes. The introduced model was then verified using full-scale experiments for beam specimens repaired using fiber-reinforced polymer laminates. The study concluded that in all experiments, the failure took place at the steel–adhesive interface.

Da Costa Mattos et al. (2014) studied the use of glass fiber–reinforced polyurethane as a repair material for corroded steel pipelines with impaired serviceability conditions. The study investigated the impact of the higher temperature on the proposed repair approach using tensile and burst experiments. Based on these investigations, the authors presented a methodology to estimate a reinforced specimen's failure pressure with arbitrary localized corrosion damage.

Elchalakani (2016) and Elchalakani et al. (2017) experimentally investigated the effect of rehabilitation corroded steel circular hollow sections using carbon fiber–reinforced polymers (CFRP). Three-point bending and direct indentation experiments were conducted. Various corrosion severities and different numbers of CFRP layers were investigated. The study found that the average possible increase in the load-carrying capacity was 97%.

Mazurkiewicz et al. (2017) presented experimental and numerical burst pressure evaluation of the gas seamless hot-rolled steel pipes wrapped with composite sleeves. The study concluded that the local reduction of pipe wall thickness due to corrosion could reduce the pipes' high-pressure resistance by about 40%; however, using fiberglass sleeves with epoxy resin on corroded pipes can turn out more burst pressure than the original steel pipe. Zhang et al. (2020) introduced theoretical expressions that can be used to quantify the debonding failure of the corroded pipe repaired with CFRP under tension and bending, with a modification of stresses using the residual strength factor. Finite element models and experimental tests were also conducted to verify the theoretical derivation, and a good agreement between the models and tests and the theoretical expressions was found.

George et al. (2021) introduced a pilot experimental study on corroded steel tubular members repaired with fiber-reinforced polymers under the

combination of axial compression and bending loads. The study included specimens repaired in air and underwater. The study also presented a finite element model that can predict the behavior of the repaired tubular members. The study found that repairing corroded steel tubular members using fiber-reinforced polymers can significantly enhance the members' axial and bending strength.

Martinez et al. (2021) introduced numerical and experimental investigations on the effectiveness of using carbon, glass fibers, and epoxy resin hybrid composite material to repair flare boom corroded tubular elements subjected to axial compressive loads. The study also determined the maximum operating temperature of the repair. It was concluded that the repaired tube's strength could exceed the intact tube capacity in many cases.

Shamsuddoha et al. (2021) introduced a finite element model of steel pipe with different corrosion levels to evaluate the grouted composite repair system's failure behavior and capacity in this study. Different corrosion levels in steel pipes that are then repaired using two infill grout systems reinforced with carbon and glass sleeves of different thicknesses were considered. The study concluded that using a high–tensile strength grout in the repair system can restore the steel pipes' capacity by 70%. Yashoda Jayasuriya (2017) and Jayasuriya et al. (2018) introduced an experimental and analytical study on the feasibility and effectiveness of using basalt fiber–reinforced polymer (BFRP) as a rehabilitation method for the steel beams. The author concluded that using BFRP can restore the corroded steel beam yield and ultimate load capacities; however, it may not be possible to restore a corroded steel beam's ductility fully.

Bastani et al. (2019) investigated the effectiveness of using the BFRP fabric as a rehabilitation method for corroded steel I-beam web. The study utilized full-scale experimental tests to validate a finite element model used to determine the best orientation and the optimum number of layers of BFRP fabric required to rehabilitate the shear-deficient steel beams. Mitra et al. (2020) investigated the feasibility of utilizing the BFRP in rehabilitating steel beams with various corrosion shapes. The study used experimental and finite element approaches to obtain a design equation that can be utilized to quantify the optimum number of BFRP layers required to completely restore the ultimate load capacity of the steel beams corroded with various shapes.

Pham et al. (2021) investigated the effectiveness of using carbon fiber–reinforced plastic sheets to repair the corroded gusset plate connections in the steel truss bridges. The study showed using experimental tests that the introduced repair approach can efficiently recover the capacity and improve the corroded gusset plate connections' deformation performance. Finite element models were then presented to validate the experiments with and without the carbon fiber–reinforced plastic sheets.

1.4 Objectives and Approach

The main objective of this investigation is to evaluate the use of fiber-reinforced polymers (FRP) as a viable repair technique for corroded members of hydraulic steel structures. This effort will be achieved by the following steps:

1. Develop numerical experiments of a horizontal frame miter gate plate girder.
2. Assume different levels of section loss on the shear and bending zones of the girders.
3. Evaluate different FRP repair schemes.
4. Evaluate the effectiveness of the repairs for the different levels of section losses.

1.5 Deterioration Plan

Corrosion can occur in multiple locations of structural elements. There are critical zones along a beam where corrosion can cause structural failure as a consequence of dramatic reduction in sectional area. The study is focusing on two zones to apply deterioration and three stress states to evaluate the loss in stiffness (increase of stress levels). The zones are where maximum shear stresses and maximum tensile stresses occur. Because the compression zone is attached to the gate's skin plate, the corrosion effect is less critical in the sense that the skin plate provides an extra section to resist the compression stresses. In an actual girder of a hydraulic structure, the forces are distributed from the water pressure and the other elements attached to it. Also, the displacement boundary conditions are closer to a fix-end condition, which reduce the stresses. To simplify the modeling and analysis, the model consisted of a simply supported girder with applied loads at third points.

A typical corrosion behavior is pitting corrosion (Kayser and Nowak 1989), where localized holes are produced on the surface, going deep into the metal. However, modeling this behavior is somewhat difficult. The corrosion in this study is modeled as a predetermined level of section loss. The study considered 10% and 25% reduction in section thickness at the shear region (near the supports). Additionally, 40% loss in section was considered for flexural deterioration in the tensile flange at the center of the girder. Preliminary analyses considered a maximum of 50% section loss. However, this level of deterioration may leave the section in an unrepairable state, and the best option is to replace or rebuild. The original section is 0.5 in.,* having final thicknesses of 0.45 in. for 10% loss, 0.375 in. for 25% loss, and 0.30 in. for 40% loss.

In simply supported beams, the maximum shear stress occurs at the web near the supports. This deterioration also translates in loss of bearing capacity. Figure 3 shows the zone over the support where deterioration of the web was investigated. This zone is where all the bearing forces are transmitted to the support and where the maximum shear stresses are at the web. The web is 50 in. tall. The section has two longitudinal stiffeners, each located at approximately a third of the height of the girder. The two panels from the support side will be deteriorated as indicated in the figure. The deteriorated area extends 50 in. in the longitudinal direction, a distance equal to one web height.

* For a full list of the unit conversions used in this document, please refer to *US Government Publishing Office Style Manual*, 31st ed. (Washington, DC: US Government Publishing Office, 2016), 345–47, https://www.govinfo.gov/content/pkg/GPO-STYLEMANUAL-2016/pdf/GPO-STYLEMANUAL-2016.pdf.

Figure 3. Web deterioration shear zone over support.

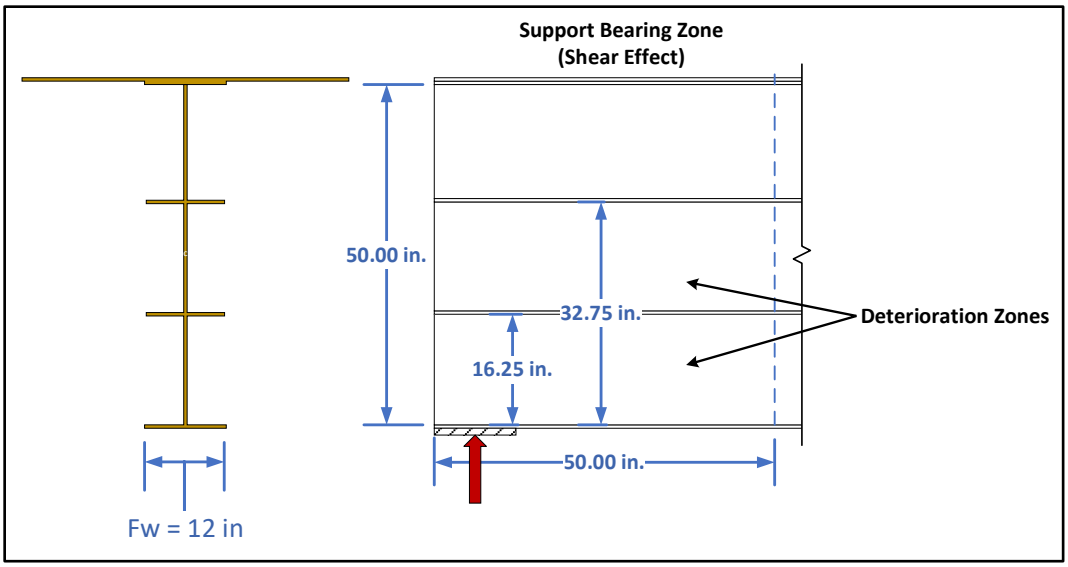

Deterioration that affects bending occurs at midspan, where the moment is maximum. Four zones of flange deterioration are defined as a function of the flange width (Fw). The flange width is 12 in. Figure 4 shows only the segment between the load application points of the girder at midspan. The length of the segment of the bottom (tensile) flange is shown in terms of number of flange widths.

Figure 4. Flexural deterioration zones of flanges at midspan.

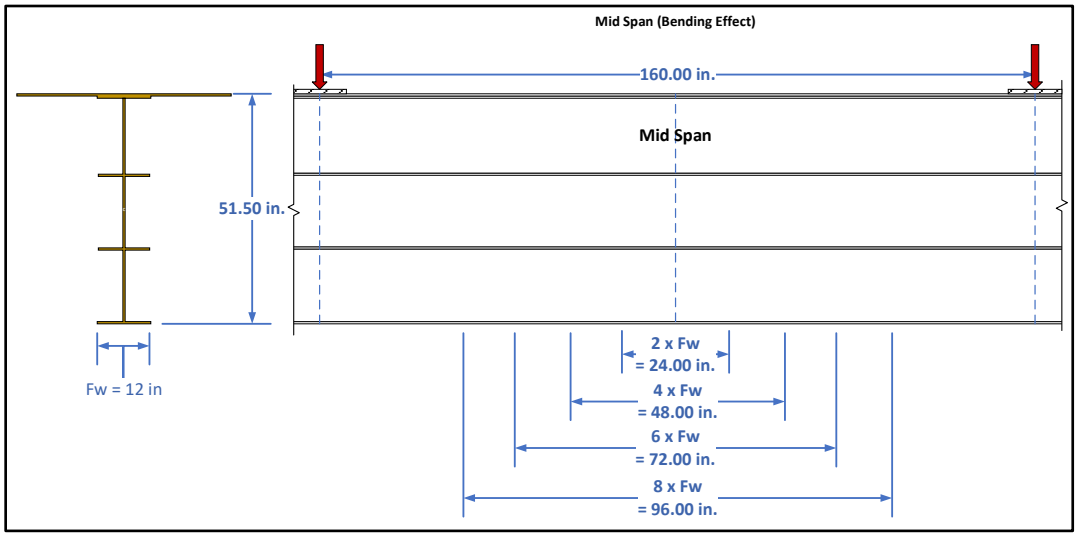

2 Finite Element Model

A finite element model using shell elements was assemble using ABAQUS (Dassault Systèmes 2015). Details of the model, including geometry, materials characteristics , displacements and loads boundary conditions, and used mesh are shown hereafter.

2.1 Basic Geometry

The girder was modeled as a simply supported four-point bending beam with an a/d ratio of 3.2, where a is the distance between the support to the load and d is the depth of the girder. Figure 5 shows the overall dimension and load location of the beam. The beam was divided into one-third lengths. The total length of the girder was 480 in. (40 ft), and each segment was 160 in. (13.33 ft).

Figure 5. Overall dimensions of the beam and third-point loading and supports are defined.

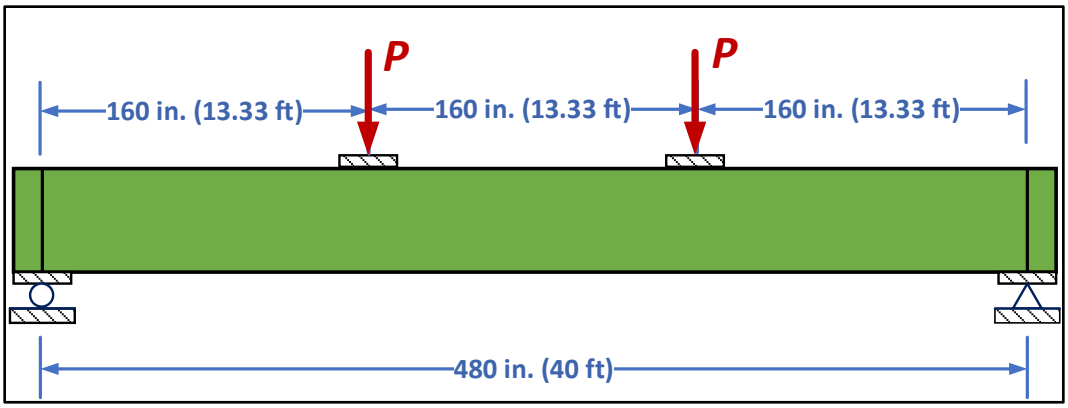

The typical cross-section of the beam is shown in Figure 6. This section includes the skin plate, using an effective width of 48 in. The overall height is 51.5 in., and subtracting the thicknesses of the two flanges and the skin plate gives a web height of 50.0 in. The girder has two longitudinal stiffeners that are located approximately at one-third height points. The flanges are 12 in. wide (Figures 3 and 4), and the longitudinal stiffeners are 5.5 in. wide (total width).

Figure 6. Typical girder cross-section.

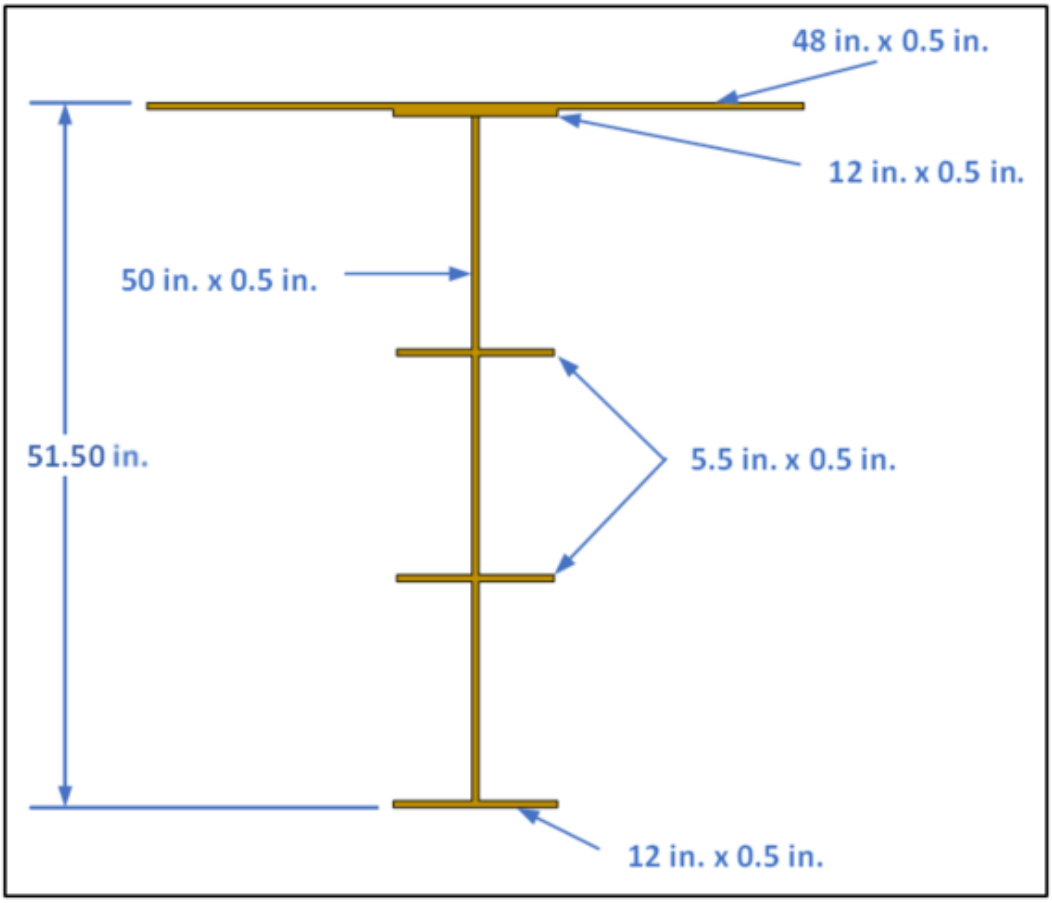

2.2 Material Properties

2.2.1 Steel Girder

The stress-strain curve of the steel used for the girder is shown in Figure 7. It was defined as elastic-perfectly plastic, with 50 ksi yielding strength. Although the analysis was conducted in the elastic range, plastic analysis was conducted to verify yielding initiation loading and to correlate with hand calculations.

Figure 7. Steel ideal stress-strain curve.

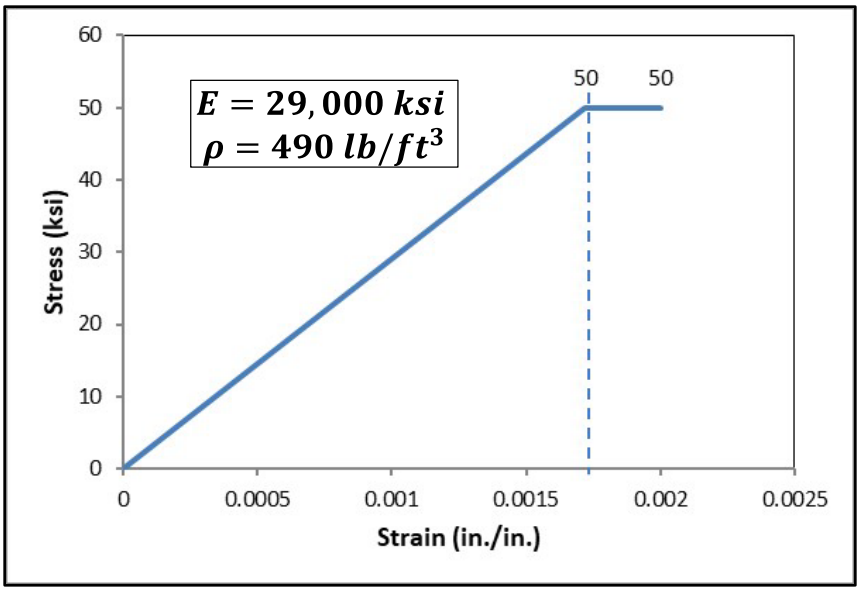

2.2.2 Carbon Fiber–Reinforced Polymer

Two material properties were used for the analysis of the repaired girder: equivalent isotropic material and orthotropic lamina to evaluate several laminate layups.

The equivalent isotropic properties, elastic modulus (E), Poisson's ratio (ν), mass density (γ, slugs), and layer thickness (t_i) are:

$$E = 11.89 \times 10^6 \text{ psi}, \nu = 0.40, \gamma = 1.63 \times 10^{-10} \text{ slugs}, t_i = 0.0628 \text{ in.}$$

These properties were estimated from the manufacturer data sheet assuming homogeneous material.

An actual composite layup involves the determination of the orthotropic properties of a single lamina, then defining different layup of fibers in a symmetric pattern to avoid twisting based on the intended application. Micromechanics (rules of mixtures [ROM]) and the information provided by the manufacturer for a single-layer mechanical property and for mechanical properties of the resin and fibers were used to backcalculate the fiber volume fraction of a lamina (v_f). Then the ROM was used to establish the lamina properties using the calculated parameters. The lamina was defined in Abaqus as orthotropic material. Then, stacking sequences were defined and applied to the defined critical zones of the model.

The ROM basic mechanics equations are (Barbero 2010; Gibson 2016) the following:

$$E_1 = E_f v_f + E_m(1 - v_f) \quad (1)$$

$$\frac{1}{E_2} = \frac{v_f}{E_f} + \frac{(1-v_f)}{E_m} \quad (2)$$

$$\frac{1}{G_{12}} = \frac{v_f}{G_f} + \frac{(1-v_f)}{G_m} \quad (3)$$

$$\nu_{12} = v_f v_f + \nu_m(1 - v_f) \quad (4)$$

where:

E_1 = modulus in the longitudinal direction of the lamina (parallel to the fibers),
E_2 = modulus in the transverse direction of the lamina (perpendicular to the fibers),
G_{12} = in-plane shear modulus of the lamina,
ν_{12} = in-plane Poisson's ratio of the lamina,
E_f = elastic modulus of the fiber,
G_f = shear modulus of the fiber,
ν_f = Poisson's ratio of the fiber,
E_m = elastic modulus of the matrix (resin),
G_m = shear modulus of the matrix (resin),
ν_m = Poisson's ratio of the matrix (resin),
v_f = fiber volume fraction of the lamina.

Because these equations depend on the value of v_f, this value was backcalculated using Equation 1 and the values of the design tensile elastic modulus provided by the manufacturer in their data sheet for the principal fiber direction. The manufacturer also provides information for the carbon fiber and epoxy resin tensile modulus. Their values are shown in Table 1. Although carbon fibers are not isotropic, they were assumed as isotropic to determine shear modulus using typical Poisson's ratio values from Barbero 2010. The estimated value of v_f of a lamina was 40%. Then, using the properties in Table 1 and Equations 2, 3 and 4, the principal lamina mechanical properties were calculated. Their values are reported in Table 2. The manufacturer also reports a nominal layer thickness of 0.04 in.

Table 1. Carbon fibers and epoxy resin properties used in rules of mixture calculations.

Property	Carbon Fibers	Epoxy Matrix
E (psi)	33.4×10^6	4.61×10^5
*G (psi)	13.9×10^6	1.67×10^5
v	0.20	0.38

* Estimated as isotropic $G = E/2(1+\nu)$

Table 2. CFRP estimated lamina properties to use in Abaqus model.

Property	Value
E_1 (psi)	13.9×10^6
E_2(psi)	7.61×10^5
G_{12} (psi)	2.76×10^5
v_{12}	0.30
t_i (in.)	0.04

2.2.3 Laminate Layup for Shear Zone Repair

To be able to properly reinforce the deteriorated shear zone, fibers must be arranged in multiple directions because of the variations in stresses that occur in the zone. Figure 8 shows an illustration of the stress flows of principal stresses in a beam along the web. Shear stresses are maximum at the support. However, the principal stresses are in tension (solid lines) and in compression (dotted lines). The flow of stresses changes along the length of the beam, turning horizontal toward midspan, where the shear goes to zero and bending is maximum. To be able to satisfy multiple stress flows, multiple fiber directions must be considered to cover the changing directions of the stresses. The schemes considered are one, two, and three layers of the isotropic equivalent CFRP. The naming used for these models are CFRP for one layer, 2-CFRP for two layers, and 3-CFRP for three layers. In addition, the estimated lamina properties were used in five symmetric laminate layups. The names given to the layups are based on the mechanical behavior derived from the distribution of the direction of the fibers through the thickness. To be more specific, it is based on the form that the basic matrices $[A]$, $[B]$, and $[D]$ result from the layup. The layup terminology is described in Table 3. These layups are schematically shown in Figure 9 and Figure 10. Figure 9 shows a schematic of the first three layups that have the same overall thickness but with the fibers oriented based on the definitions described in Table 3. Two additional variations of

the cross-ply configurations are shown in Figure 10, having 1.5 and 2 times the number of layers in the original cross-ply layup shown in Figure 9.

Figure 8. Stress flow and principal stresses in beams. Solid lines show tensile stress directions, and dotted lines are compressive stress directions. (Adapted from Higdon et al. 1985.)

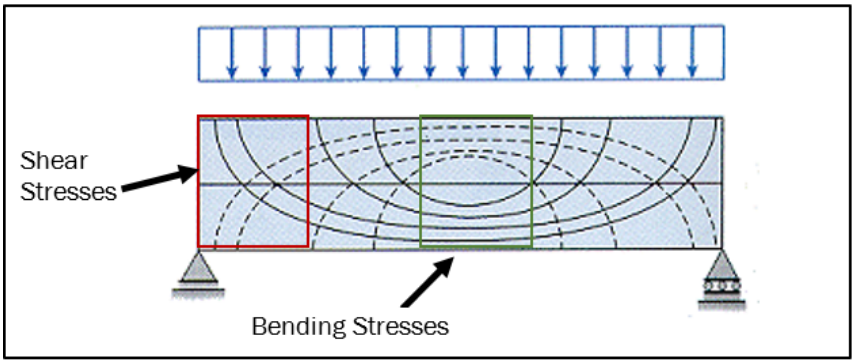

Table 3. Definition of the layups evaluated to repair the shear zone in the girder.

Name	Definition
Quasi-isotropic	Same lamina with layers equally oriented with respect to each other.
Angle-ply	Same number of plies oriented in $+\theta/-\theta$
Cross-ply	Similar to Angle-Ply but oriented specifically at 0°/90°

Figure 9. Laminate symmetric layup used in Abaqus models. The 0° fiber direction is parallel to the longitudinal axis of the beam as shown in Figure 11.

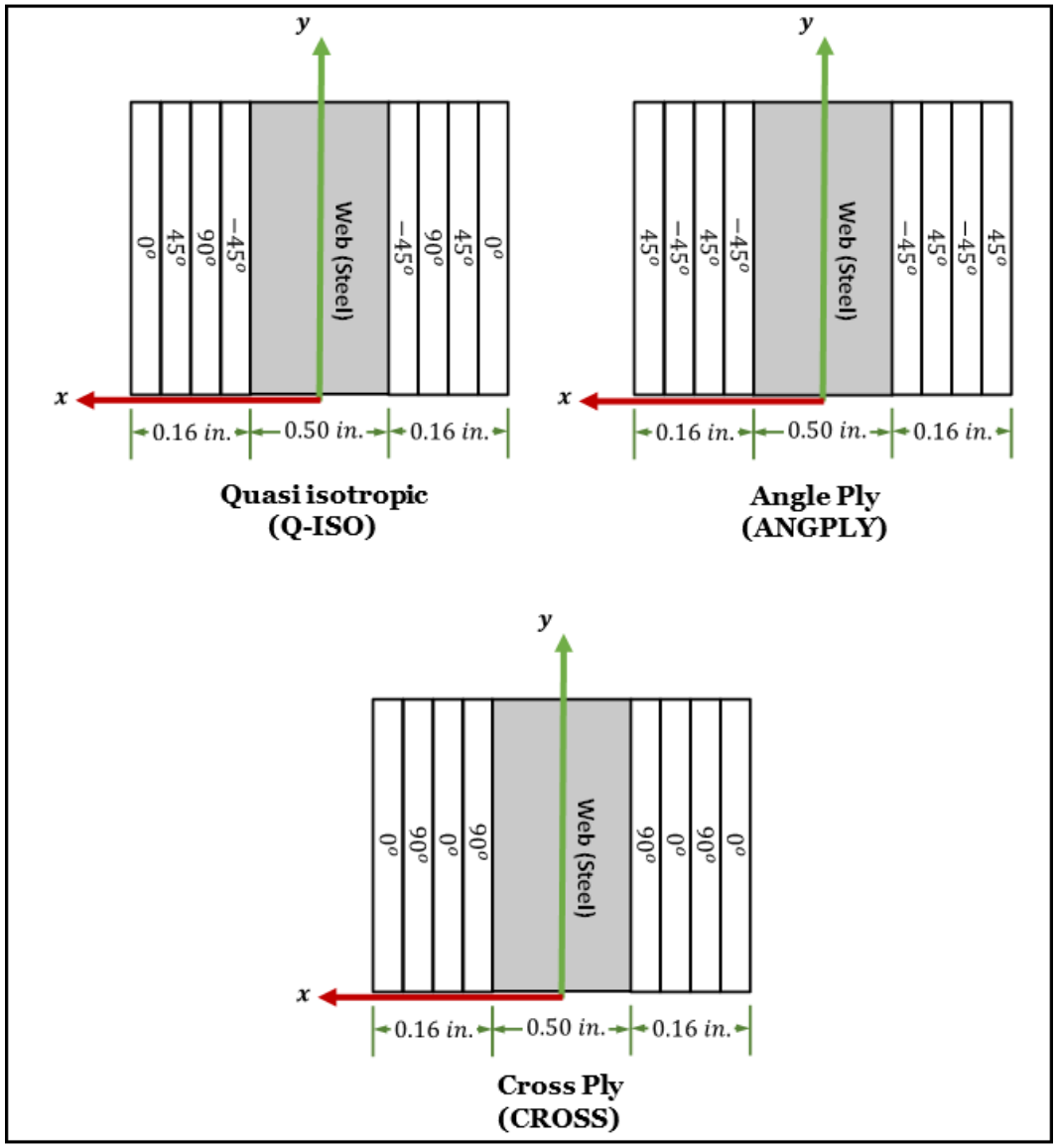

Figure 10. Two additional versions of the cross-ply laminate layup used in Abaqus models: 1.5 and 2 times the original cross-ply layup shown in Figure 9.

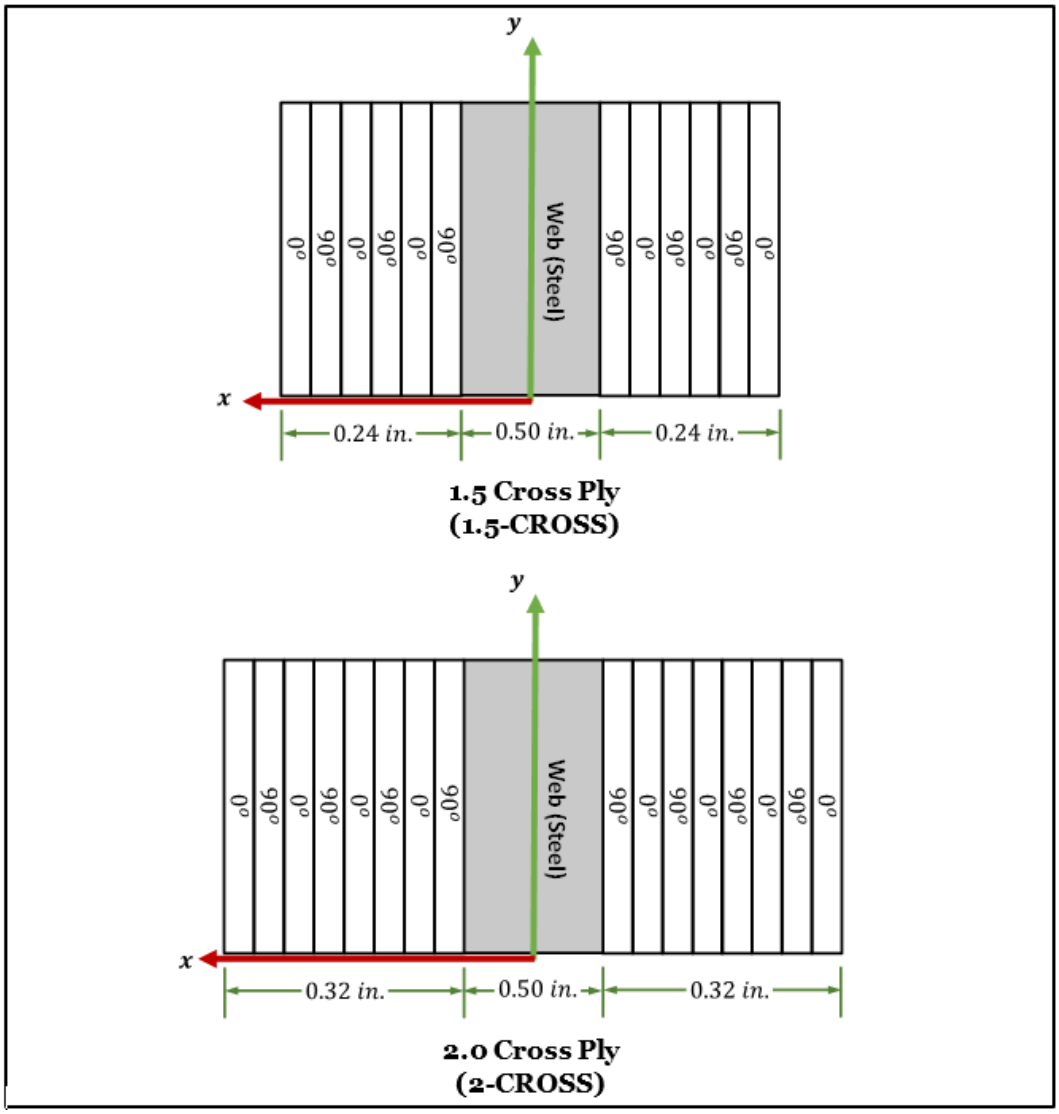

The zone to apply deterioration is shown in Figure 11. The web was deteriorated above the bearing support plate in two places in the vertical direction at one-third and two-thirds from the bottom flange. This zone is encased between the longitudinal stiffeners. The deteriorated zone extends 50 in. from the beam's edge, representing one web height. The repair scheme was applied to the entire web height but extending 1.5 times the web height from the edge of the beam in the longitudinal direction (75 in.). The figure also shows the reference angle orientation of the CFRP repair schemes shown in Figure 9 and Figure 10.

Figure 11. FRP repair zone covering the entire web height and extending 1.5 times the deterioration zone.

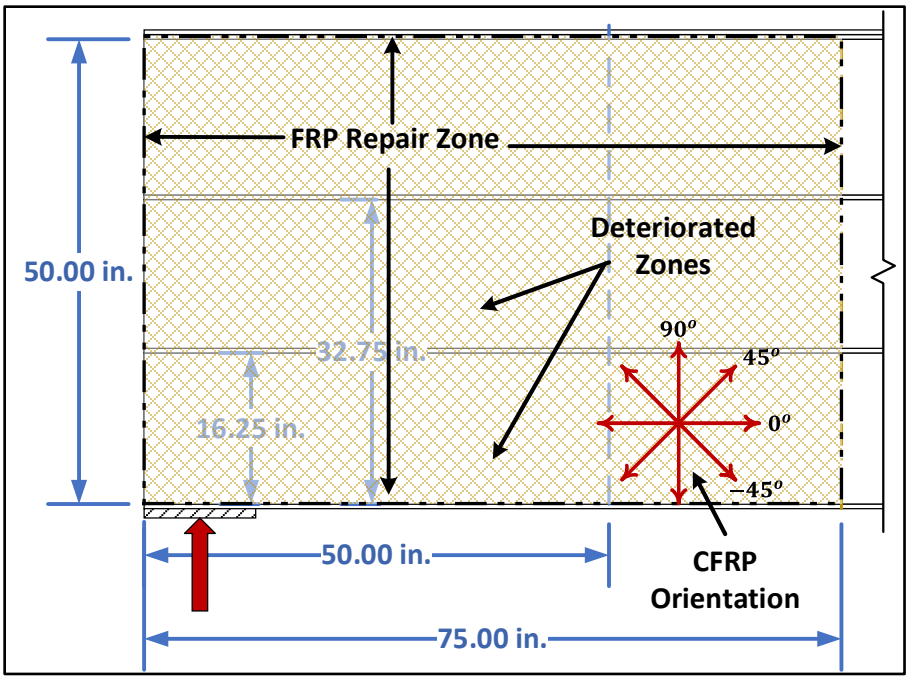

2.3 Laminate Layup for Tensile (Bending) Flange Deterioration

In the case of tensile flange deterioration (bending), because the stresses are acting only in the longitudinal direction, unidirectional layers aligned with the girder's longitudinal axis are needed. To determine the amount of layers needed to repair the corrosion damage to the bottom flange, a series of 1, 2, 3, 4 , 8, and 10 layers was evaluated. The laminate extended from loading point to loading point (only half of the model is used considering symmetry) as shown in Figure 12, covering the series of defined degradation extension lengths that were previously defined and illustrated in Figure 4. The figure also shows that the fiber principal direction (0°) is parallel to the longitudinal direction of the girder.

Figure 12. Location of the unidirectional repair applied to the bottom flange.

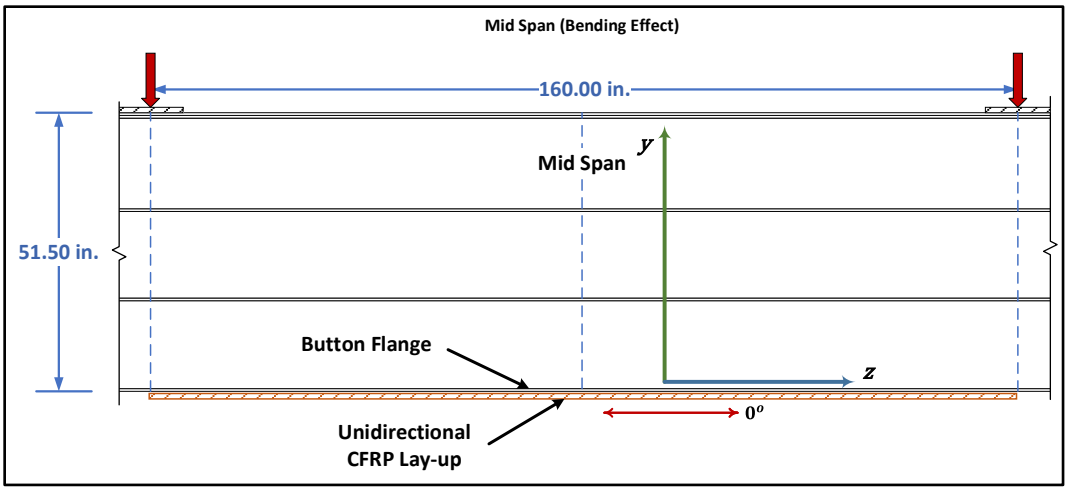

2.4 Finite Element Geometry and Mesh

The loading and support of the girder is symmetric when there is no damage. Although damage is assumed to occur in only one end of the girder, to simplify the modeling, symmetry with respect to the center of the girder was assumed and used in the development of the model. The general geometry of the model and displacement boundary conditions are shown in Figure 13. Joining of the skin plate and support bearing plate are attached using tie constraints. The loading plate is in contact with the skin plate using contact properties. The support plate and loading plate are defined as rigid elements. The rest of the model is deformable bodies with their respective material properties. The CFRP repair schemes are also quadratic shell elements. They are attached to the structure using tie constraints. Stiffeners were added to the skin plate to simulate the rigid behavior from all the transverse elements that a real gate will have between each horizontal girder.

Eight-node quadrilateral thin shell elements were used for the skin plate, girder, stiffeners, and CFRP layers. Four-node solid hexahedral elements were used for the bearing and loading plates. The total number of shell elements for all parts, not including the CFRP, was 9,440. The total number of solid hexahedral elements was 80. Figure 14 shows a portion of the model where the detail of the element mesh can be observed.

Figure 13. Features of boundary conditions, symmetric planes, and support and loading locations defined in the finite element model. General coordinate system is shown.

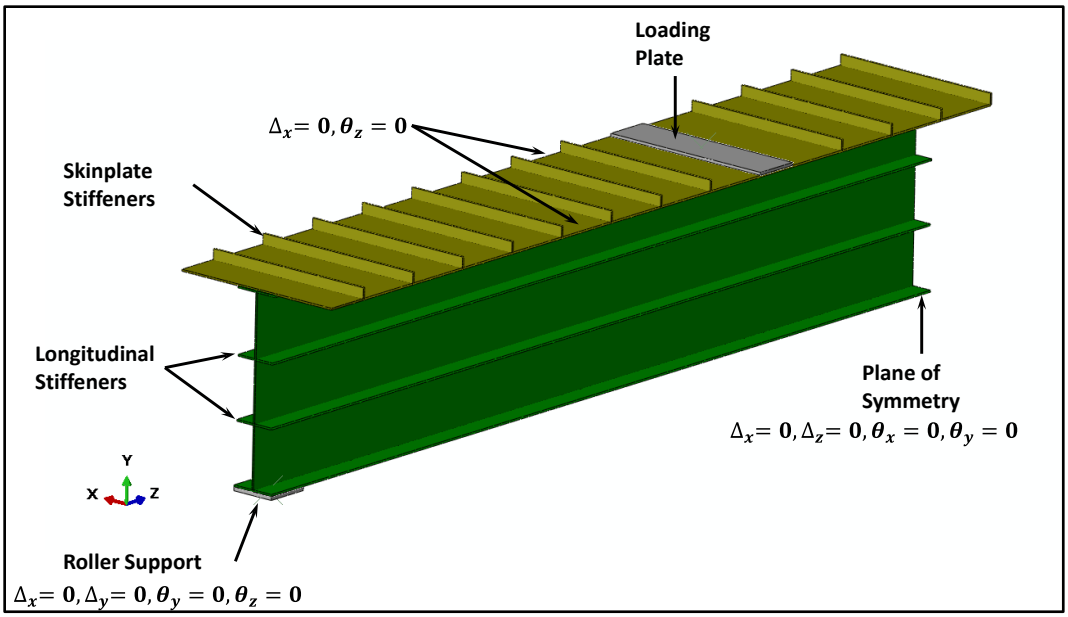

The initial analysis was divided into four analytical steps, where the load in each step was carried out to the next step. The first step was the application of the self-weight. The second step was a concentrated force at the loading plate of 175,520 lb. The third step added the remaining load to reach yielding of the bottom, tension, and flange at midspan. The load was 43,880 lb. The applied load to reach yielding was 219,400 lb. The separation of the load was for convenience because for the maximum degradation of 50%, if the full load is applied, it would have taken too many analytical increments to finish the analysis and become unstable. The last step was to go beyond yield point, adding 100,600 lb for a total of 320,000 lb.

Figure 14. Finite element mesh, quadratic shell elements for all plate sections, and solid linear elements for bearing plates of supports and loading.

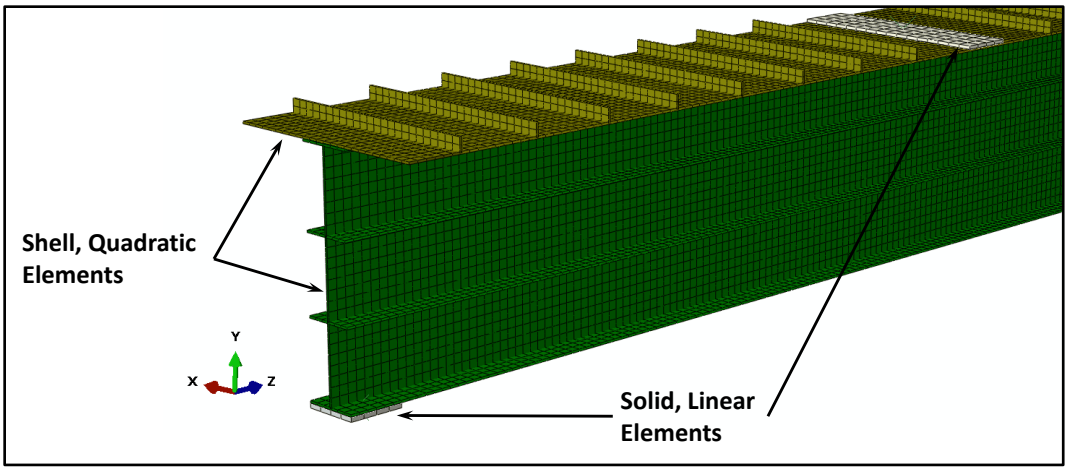

3 Analytical Results

This section presents results of the analysis performed to the model, starting with results in the nondeteriorated state, buckling analysis to evaluate the analytical limit, and the effect of deterioration and repair techniques.

3.1 Nondeterioration

A simple mechanics of material analysis was used to determine the beginning of yielding at the bottom (tension) flange of the girder at midspan where the maximum moment occurs. It was found that at approximately 219,400 lb, yield will start at the bottom flange. This load does not consider design safety factors established by AISC (2017) and US Army Corps of Engineers engineering manuals. Figure 15 shows contour maps of the longitudinal stress, having set the upper limit to the yield value of 50 ksi. The gray color represents the values of stresses that have exceeded the preimposed limit.

The applied load was increased by 100,600 lb to reach a maximum load of 320,000 lb. The analysis stopped at 318,390 lb. At this point the analysis was unstable and the increments were in the order of 10^{-5}. Figure 16 shows contours of the von Mises stresses. In the contour plots, it was observed that the web yielded up to the neutral center. Also, the compression side at the top flange was deforming considerably and yielded with higher deformation. Yielding can be observed at the bearing zone above the support.

Figure 15. Longitudinal bending stresses showing the point where yielding starts to occur at the bottom of the beam.

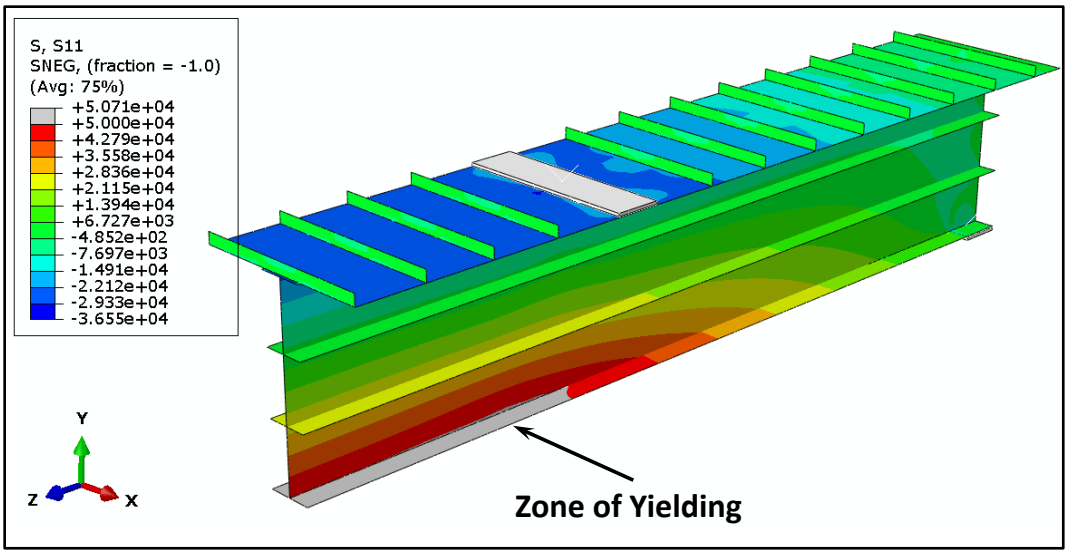

Figure 16. Von Mises stress field after reaching the limit of the analysis.

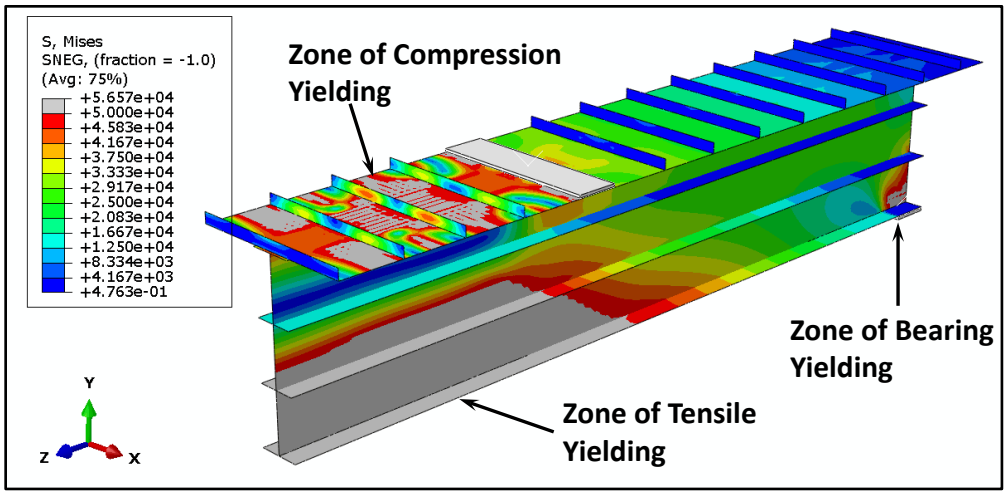

3.2 Buckling Analysis

A linear buckling analysis was performed to determine if the model configuration would be able to reach yielding before buckling. Several iterations were performed to establish the necessary elements in the model to prevent unprobeable buckling modes, such as if the load was reversed to buckle the bottom flange. The initial load applied to determine the first eigenvalue was 320,000 lb, the same load used in the static analysis. The final configuration and buckling mode resulted from the analysis is shown in Figure 17. The eigenvalue of the mode shown is 0.7766, which produces a load of 248,500 lb. This load value is larger than the 219,400 lb that was

computed as the elastic limit of the bottom flange. In other words, buckling of the web at the zone over the support will not occur prior to reaching the elastic load range.

Figure 17. First deformation mode due to buckling at compression site over the support.

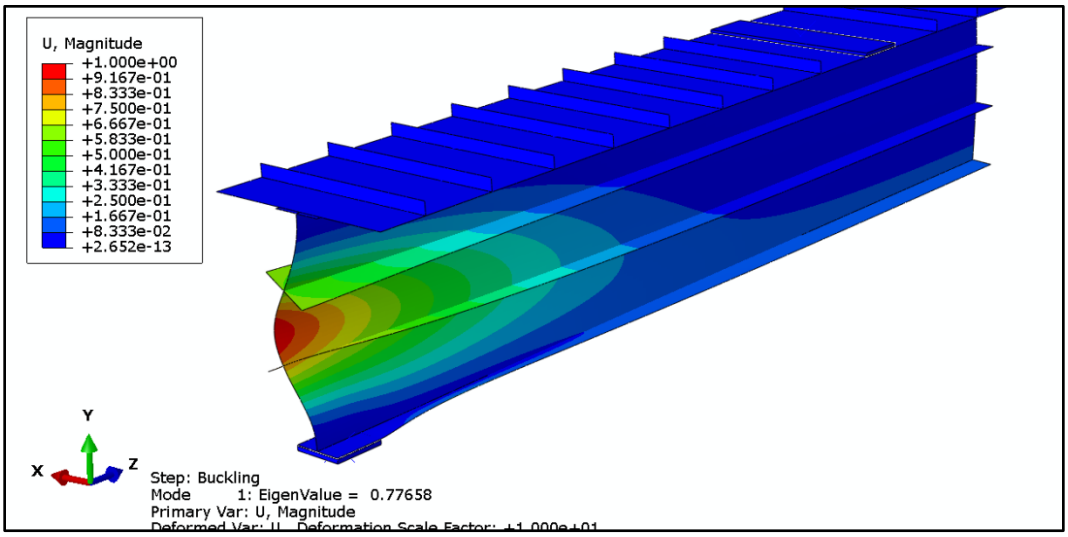

3.3 Corrosion Deterioration

This section presents the results of the analyses of the girder without deterioration, with the different levels of deterioration, and with the proposed CFRP repair schemes. Each is compared at a load below failure to determine the effectivity of the method by observing the changes in stresses at the affected zone.

3.3.1 Shear Dominated Zone

The deterioration scheme used was for 10% and 25% reduction in web section at one-third and two-thirds of the web height measured from the bottom flange (Figure 18). The 40% and 50% schemes were not performed because preliminary results showed that it was not feasible to repair beyond the 25% deterioration.

Results of the von Mises stresses were extracted from three paths located vertically on the web on top of the support where shear stresses dominate as shown in Figure 19. The paths are labeled as P_E for the end edge, P_I for the interior edge, and P_C for near the central portion based on the dimensions of the support bearing plate. The path runs from the bottom flange

up to the full height of the web plate following the element edges. The results were extracted isolating the web from the other elements of the model.

Figure 18. Illustration of the deterioration zones defined as one-third and two-thirds of the web height.

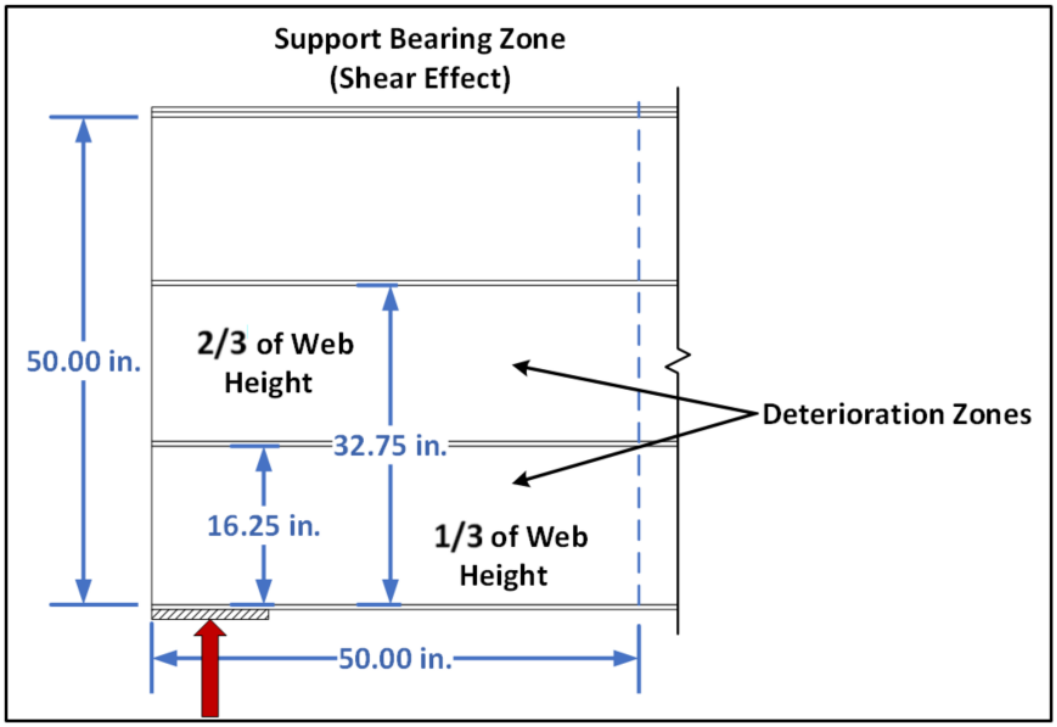

Figure 19. Path defined to extract stresses along the web height.

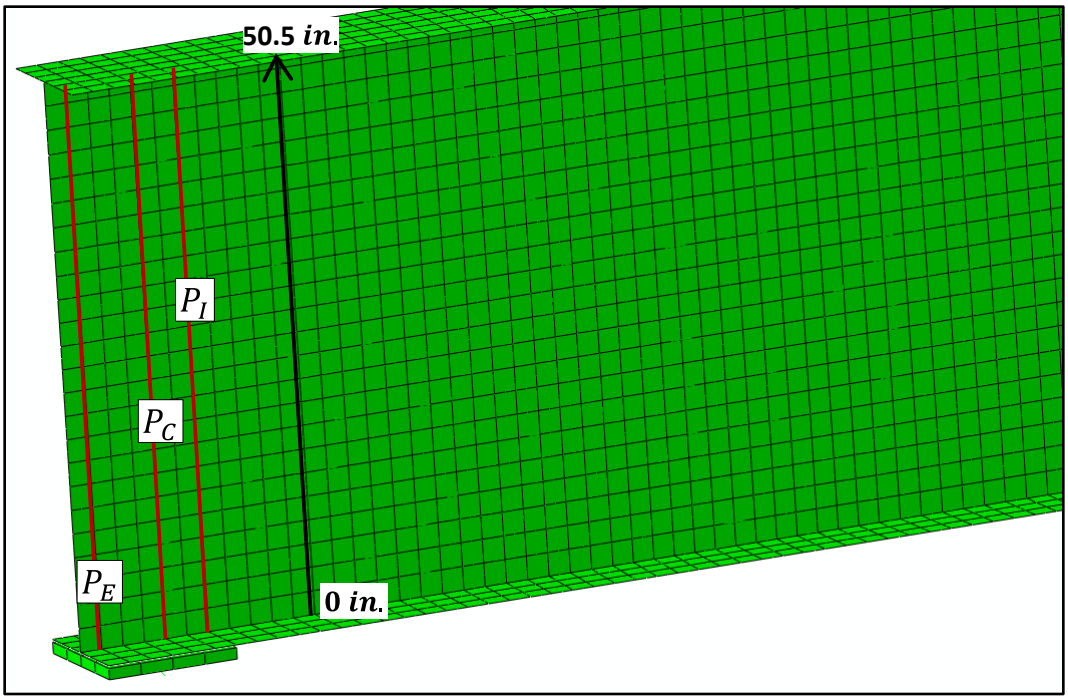

Comparison of the results of the analysis for 10% deterioration at one-third of the web height for paths P_E, P_C and P_I is shown in Figure 20 through Figure 25. The graphs show the von Mises stresses comparing the undamaged and damaged condition with the evaluated CFRP repair schemes. Figures 20–22 compare the results with the isotropic CFRP layers, and Figures 23–25 compare the results from the laminate layups. The red curve in both sets of graphs is the stresses without deterioration at the applied load of 87,760 lb. The light blue line (only in Figures 20–22) is the stresses of the deteriorated web without any repair technique. The kinks in the curves are the locations of the longitudinal stiffeners; the first one is located at 16.25 in. from the bottom flange. At the applied load, the two layers of the isotropic CFRP returned the stresses at the steel to the undamaged level (Figures 20–22). However, from the laminate layups shown in Figures 23–25, the only layup that did not reduce the stresses along the paths P_E and P_C is the ANGLPLY layup. The rest of the schemes reduced the stresses in the deteriorated steel below the undamaged condition.

Similarly, Figures 26–28 and Figures 29–31 show similar comparisons but for the deterioration from the bottom flange up to two-thirds of the web height along paths P_E, P_C, and P_I. The conclusions from these results are the same as the previous results for the one-third height shown in Figures 20–22 and Figures 23–25.

Figures 32–34 and Figures 35–37 show stresses along the paths P_E, P_C, and P_I for a deterioration level of 25% up to one-third of the web height. In Figures 32–34, none of the isotropic CFRP schemes reduced the stresses to the level of the undamaged condition. In Figures 35–37, only the repair schemes of 1.5 CROSS and 2.0 CROSS showed a reduction of stress level at the steel of the web for path P_E, but the reduction did not reach the undamaged condition for the other two paths. However, if the deterioration reaches two-thirds of the web from the bottom flange (results shown in Figures 38–40 and Figures 41–43), the repair schemes do not help to reduce the stresses at the web. Improvement occurs only very close to the bottom flange.

Figure 20. Comparison of the von Mises stresses produced along path P_E for the bottom one-third of the web with no deterioration and 10% with no carbon fiber–reinforced polymers (CFRP), one-layer CFRP, and two-layer (2-)CFRP.

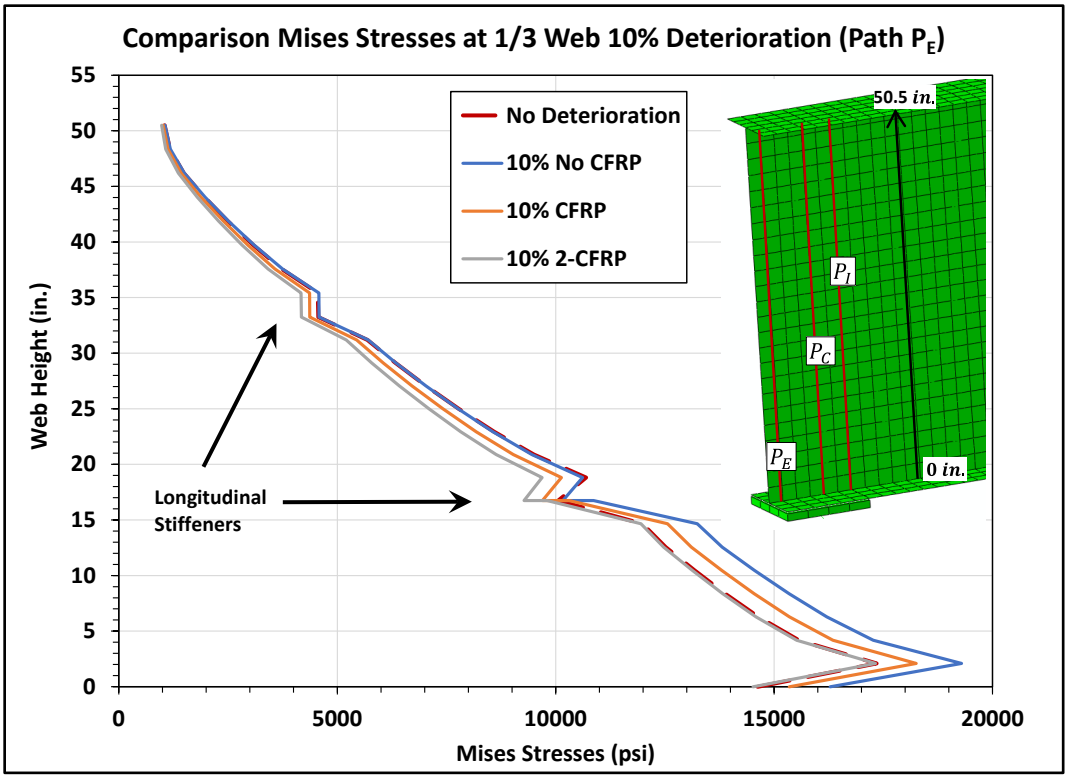

Figure 21. Comparison of the von Mises stresses produced along path P_C for the bottom one-third of the web with no deterioration and 10% with no CFRP, CFRP, and 2-CFRP.

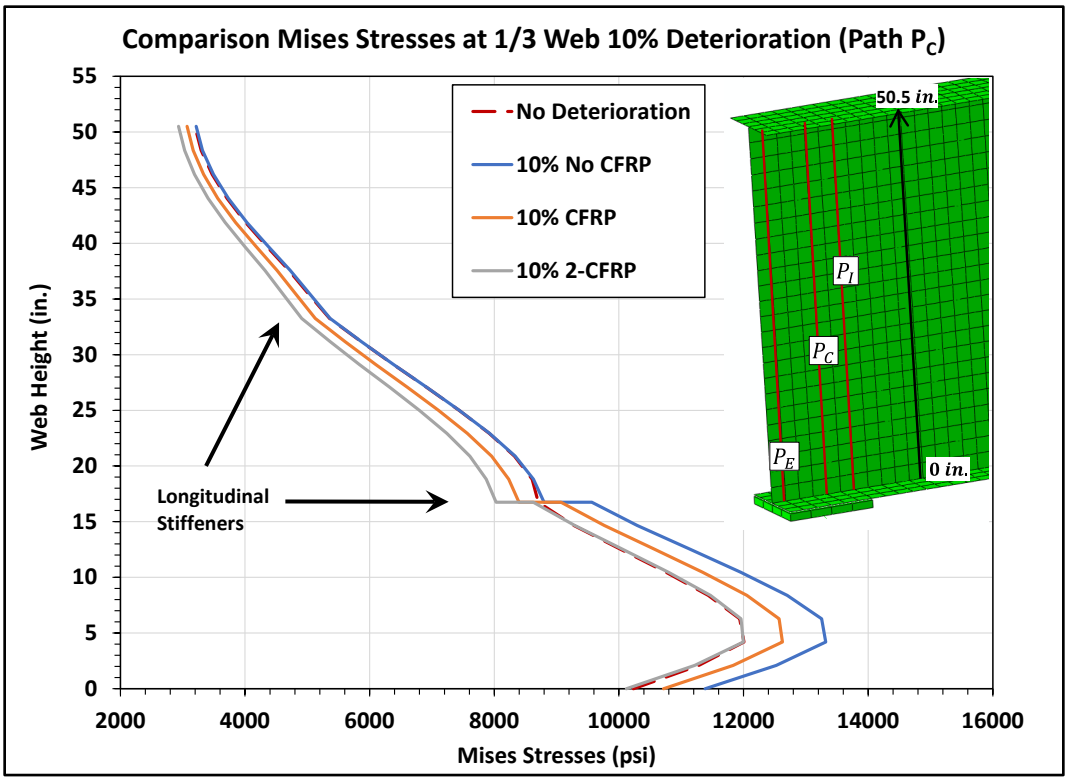

Figure 22. Comparison of the von Mises stresses produced along path P_I for the bottom one-third of the web with no deterioration and 10% deterioration with no CFRP, CFRP, and 2-CFRP.

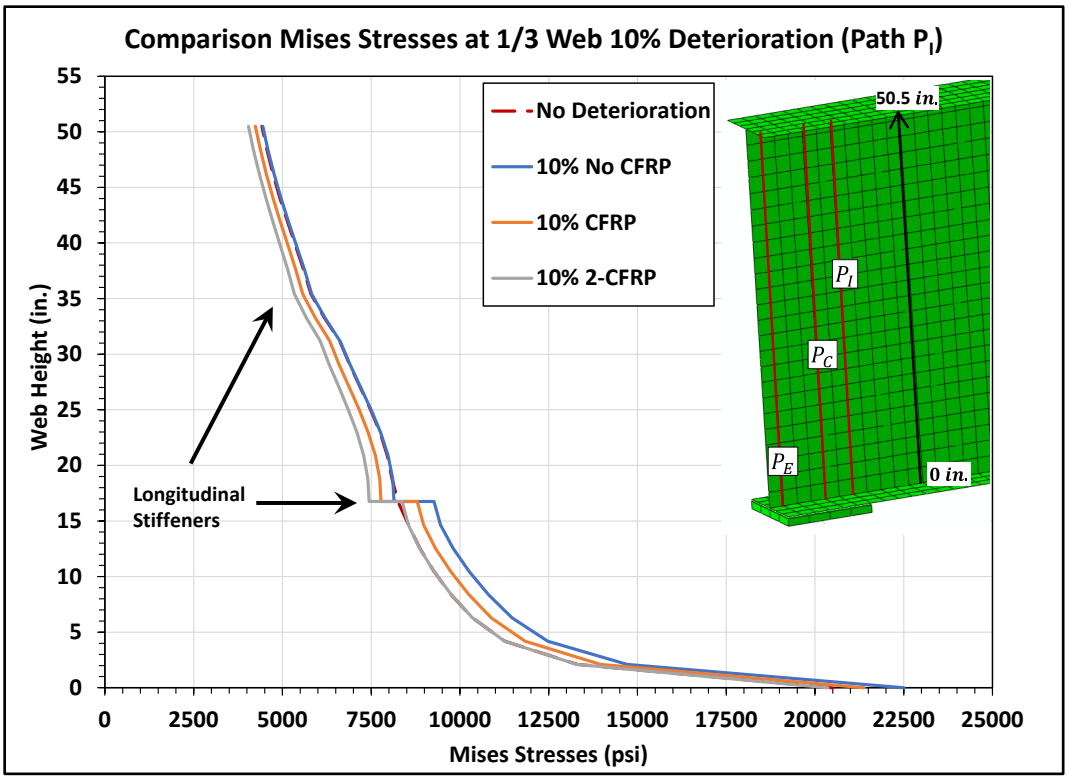

Figure 23. Comparison of the von Mises stresses produced along path P_E for the bottom one-third of the web with no deterioration and the five laminate configurations repairing the 10% deteriorated web.

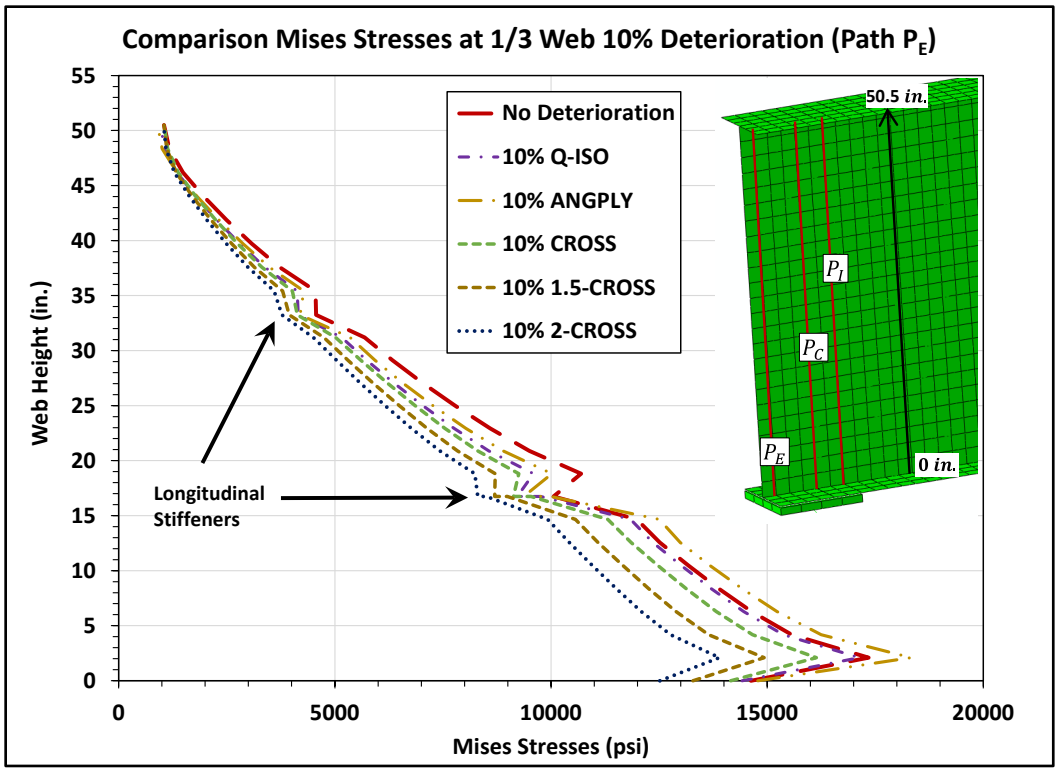

Figure 24. Comparison of the von Mises stresses produced along path P_c for the bottom one-third of the web with no deterioration and the five laminate configurations repairing the 10% deteriorated web.

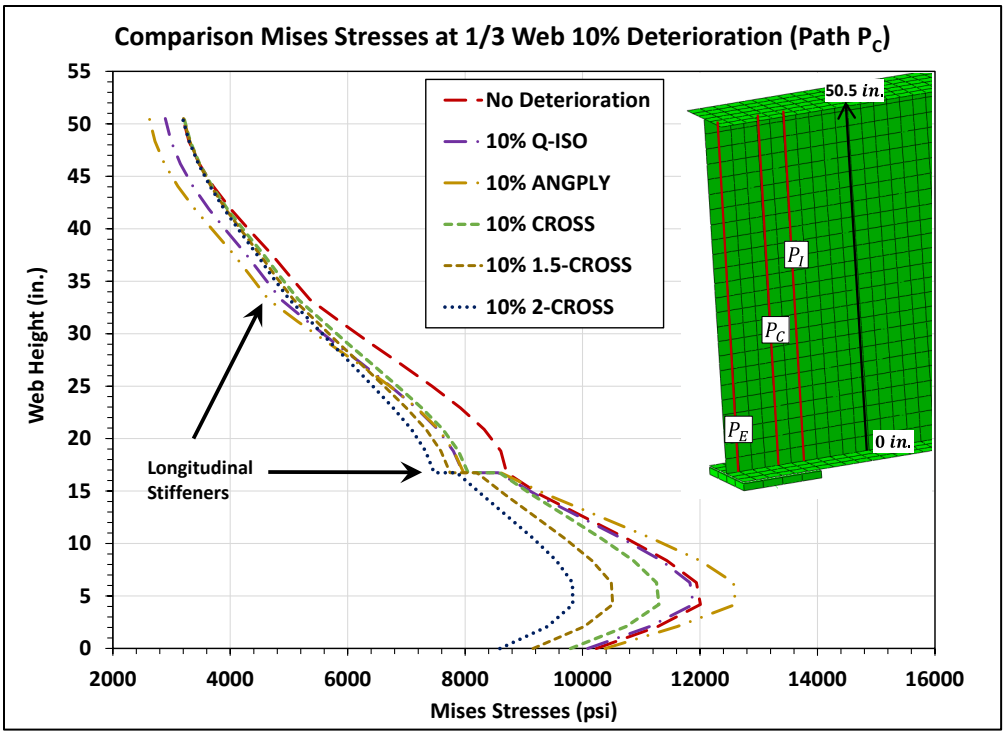

Figure 25. Comparison of the von Mises stresses produced along path P_l for the bottom one-third of the web with no deterioration and the five laminate configurations repairing the 10% deteriorated web.

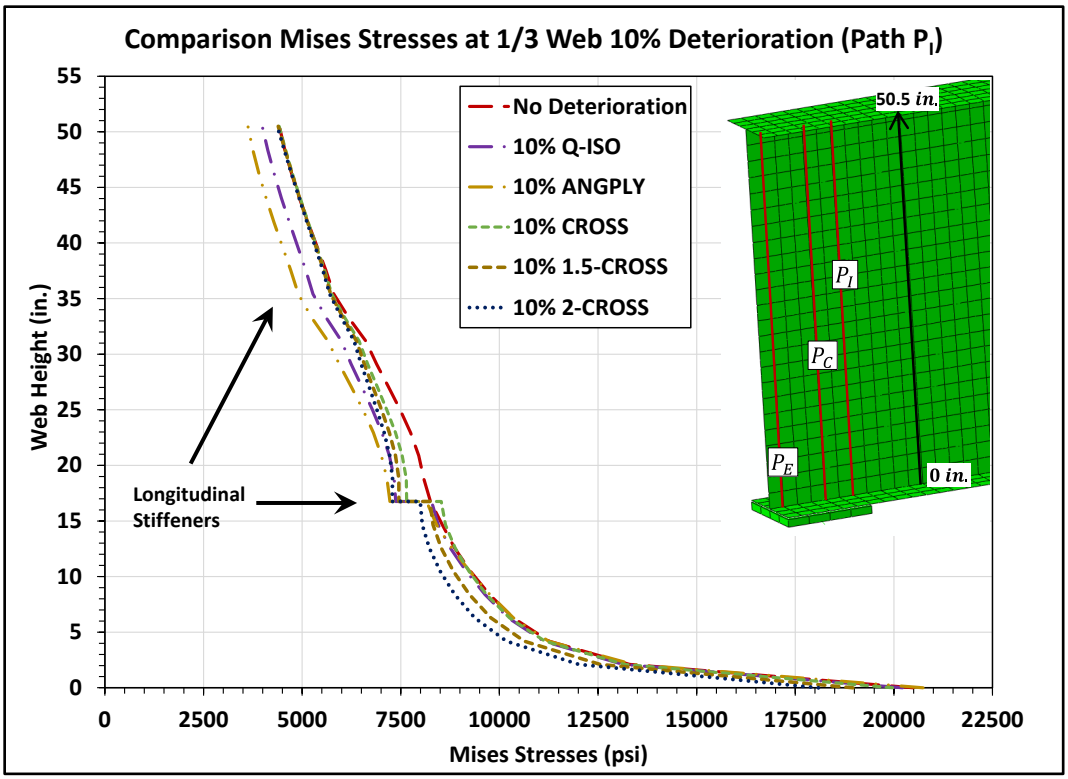

Figure 26. Comparison of the von Mises stresses produced along path P_E for the bottom two-thirds of the web with no deterioration and 10% deterioration with no CFRP, CFRP, and 2-CFRP.

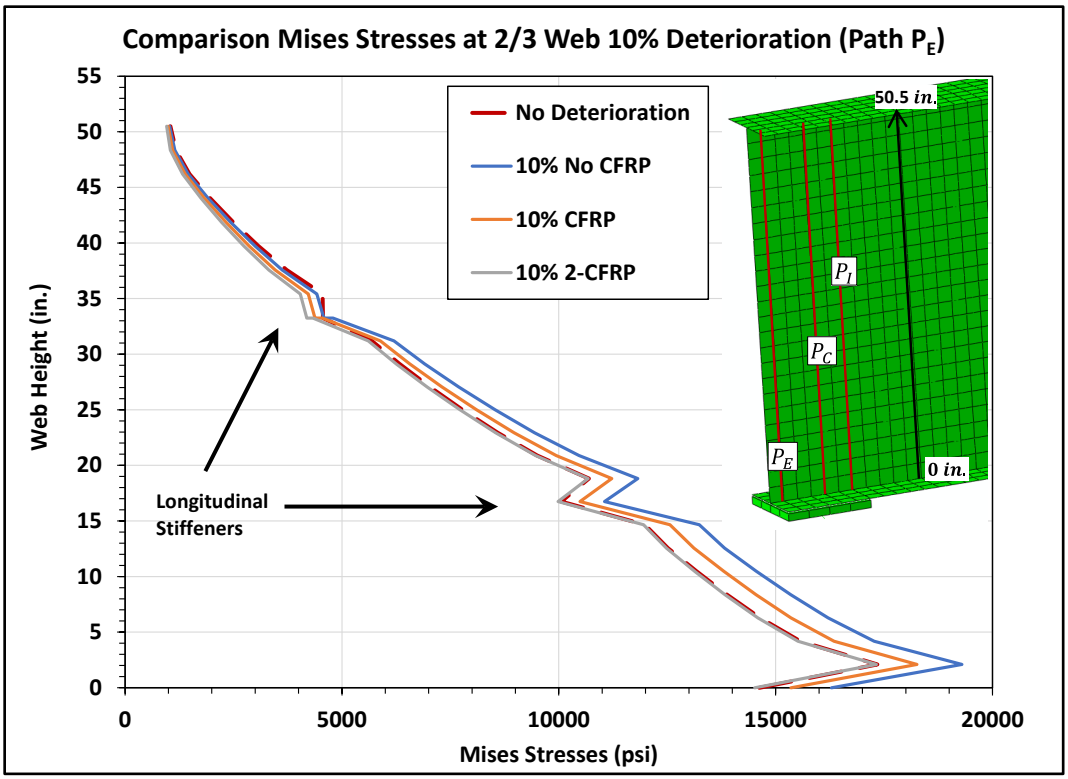

Figure 27. Comparison of the von Mises stresses produced along path P_C for the bottom two-thirds of the web with no deterioration and 10% deterioration with no CFRP, CFRP, and 2-CFRP.

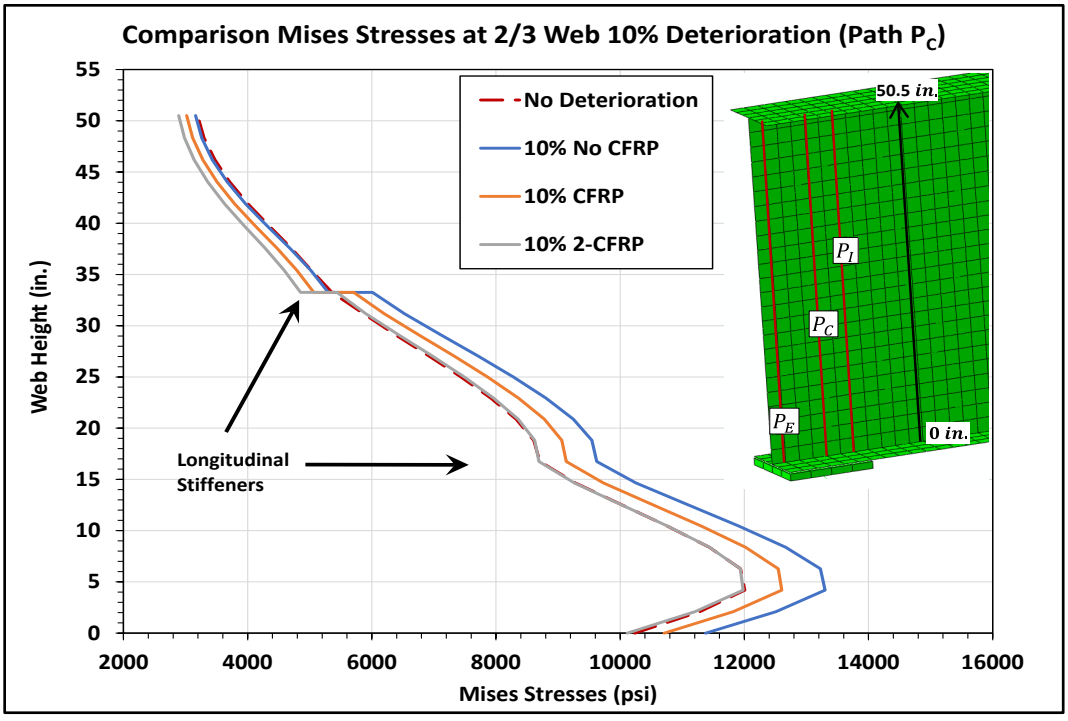

Figure 28. Comparison of the von Mises stresses produced along path P_I for the bottom two-thirds of the web with no deterioration and 10% deterioration with no CFRP, CFRP and 2-CFRP.

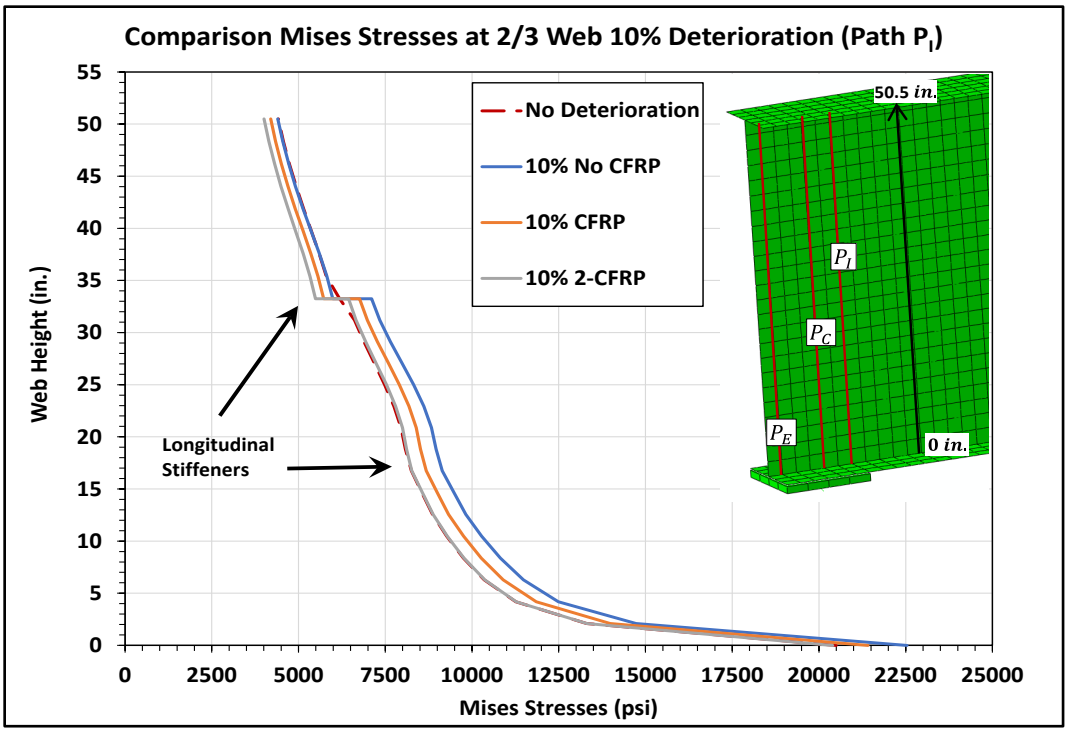

Figure 29. Comparison of the von Mises stresses produced along path P_E for the bottom two-thirds of the web with no deterioration and the five laminate configurations repairing the 10% deteriorated web.

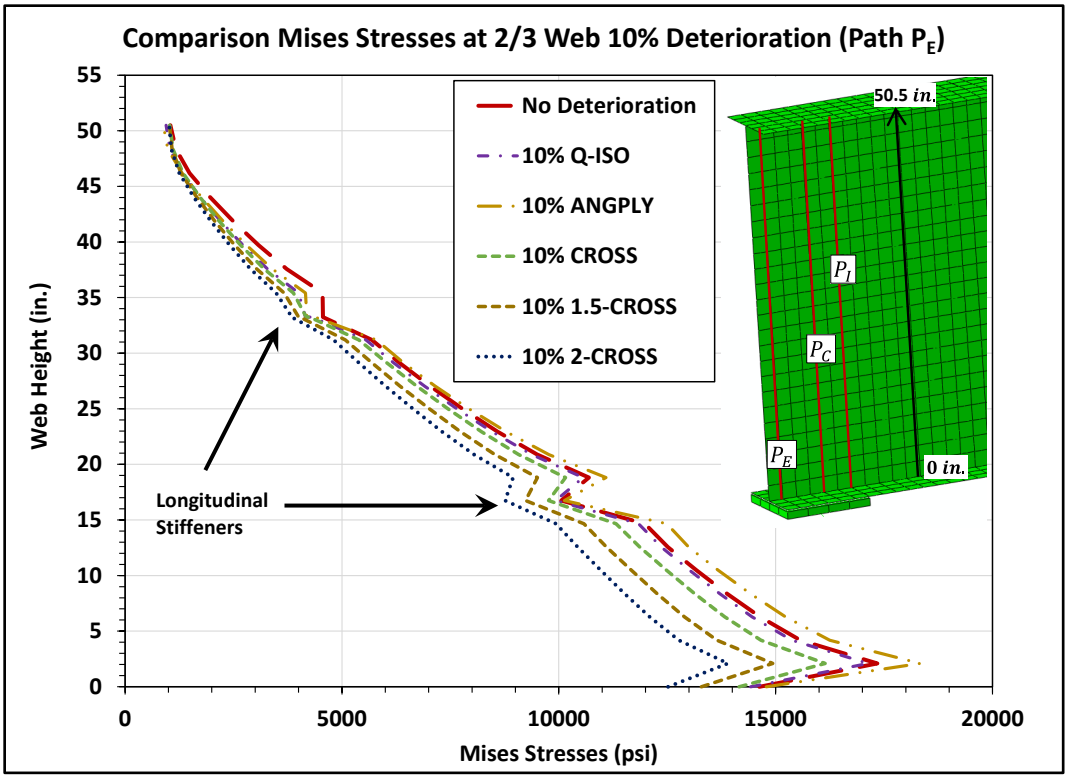

Figure 30. Comparison of the von Mises stresses produced along path *Pc* for the bottom two-thirds of the web with no deterioration and the five laminate configurations repairing the 10% deteriorated web.

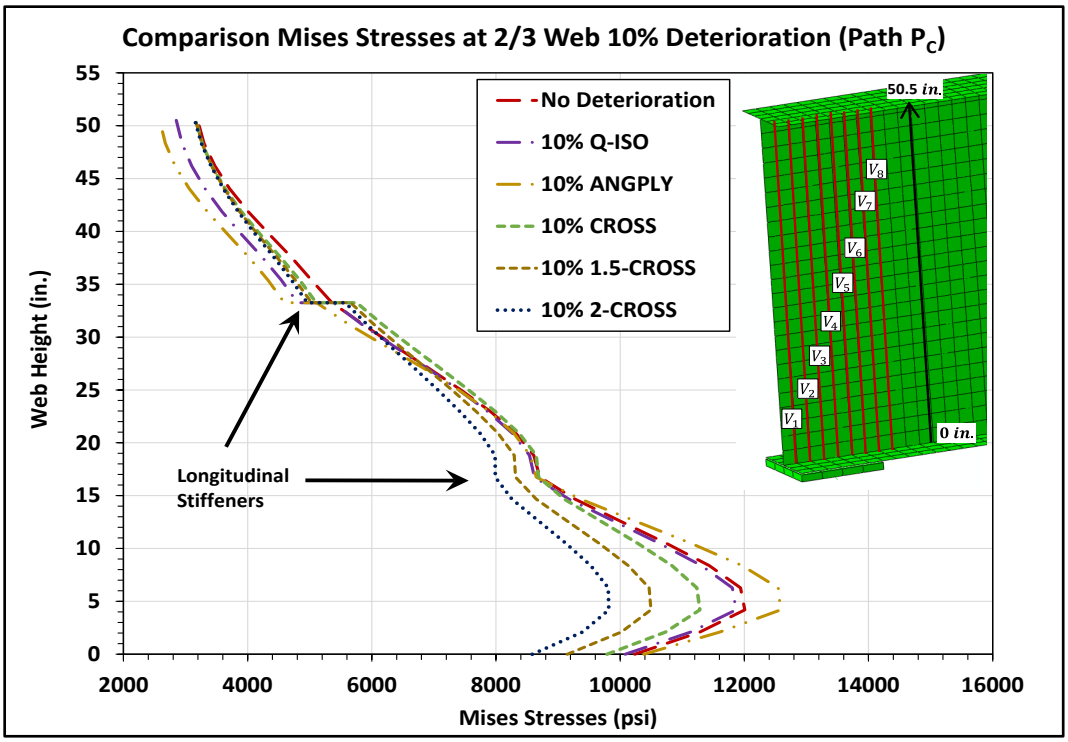

Figure 31. Comparison of the von Mises stresses produced along path *Pl* for the bottom two-thirds of the web with no deterioration and the five laminate configurations repairing the 10% deteriorated web.

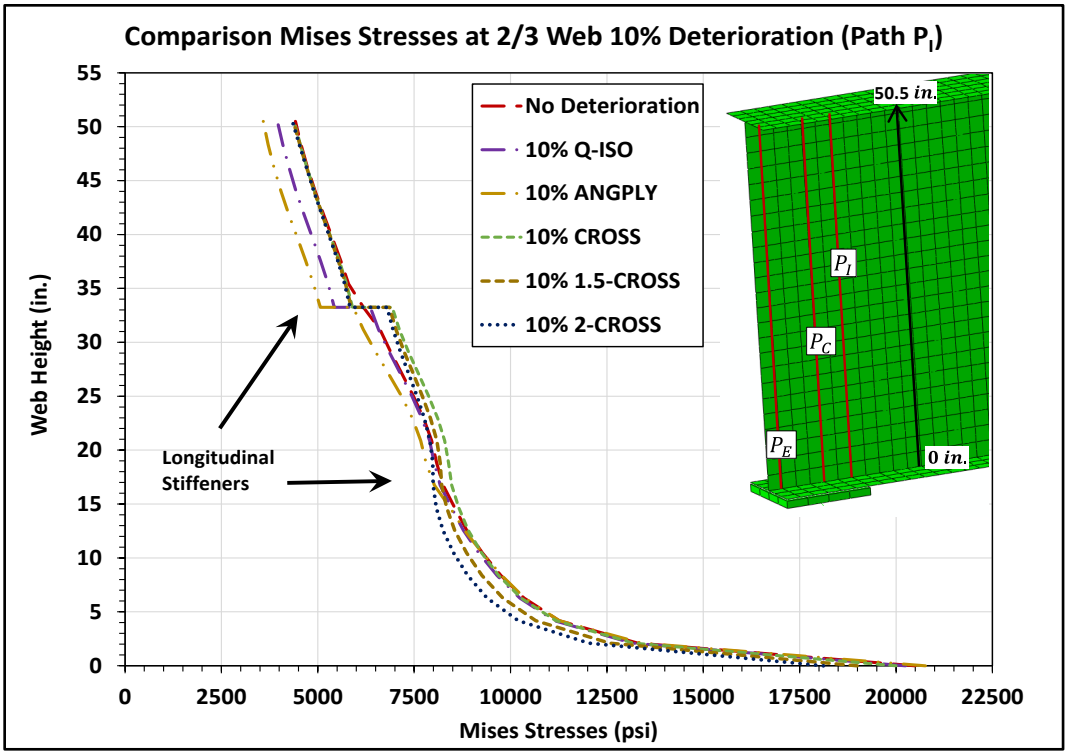

Figure 32. Comparison of the von Mises stresses produced along path P_E for the bottom one-third of the web with no deterioration and 25% deterioration with CFRP, 2-CFRP, and 3-CFRP.

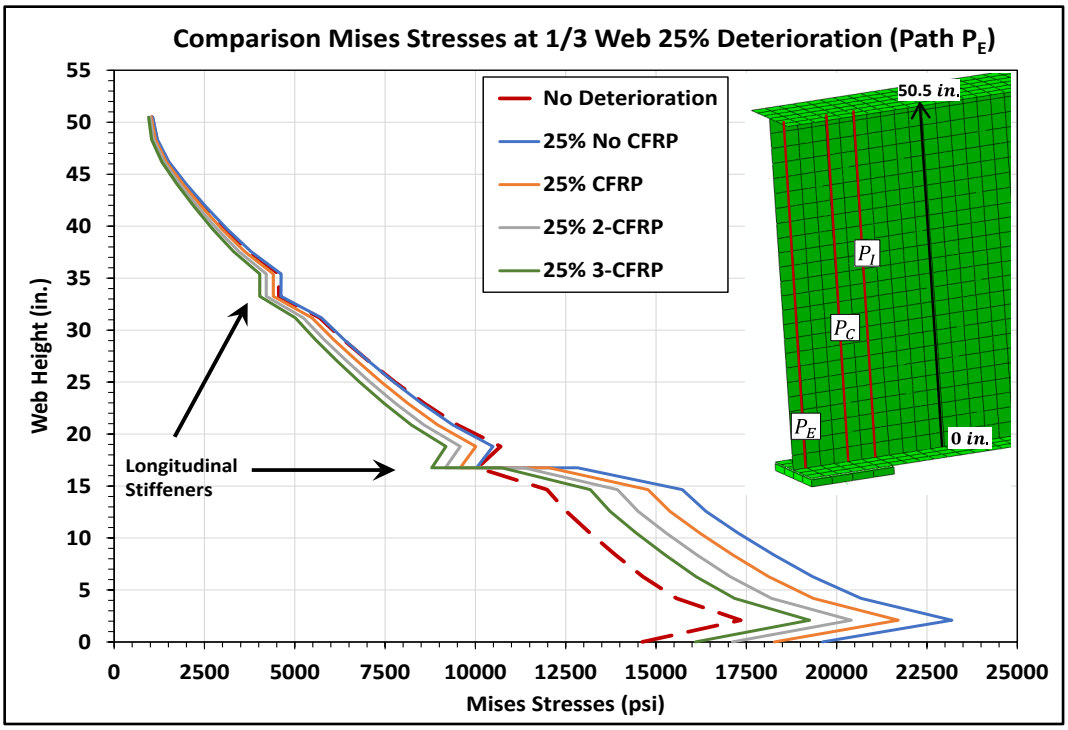

Figure 33. Comparison of the von Mises stresses produced along path P_C for the bottom one-third of the web with no deterioration and 25% deterioration with CFRP, 2-CFRP, and 3-CFRP.

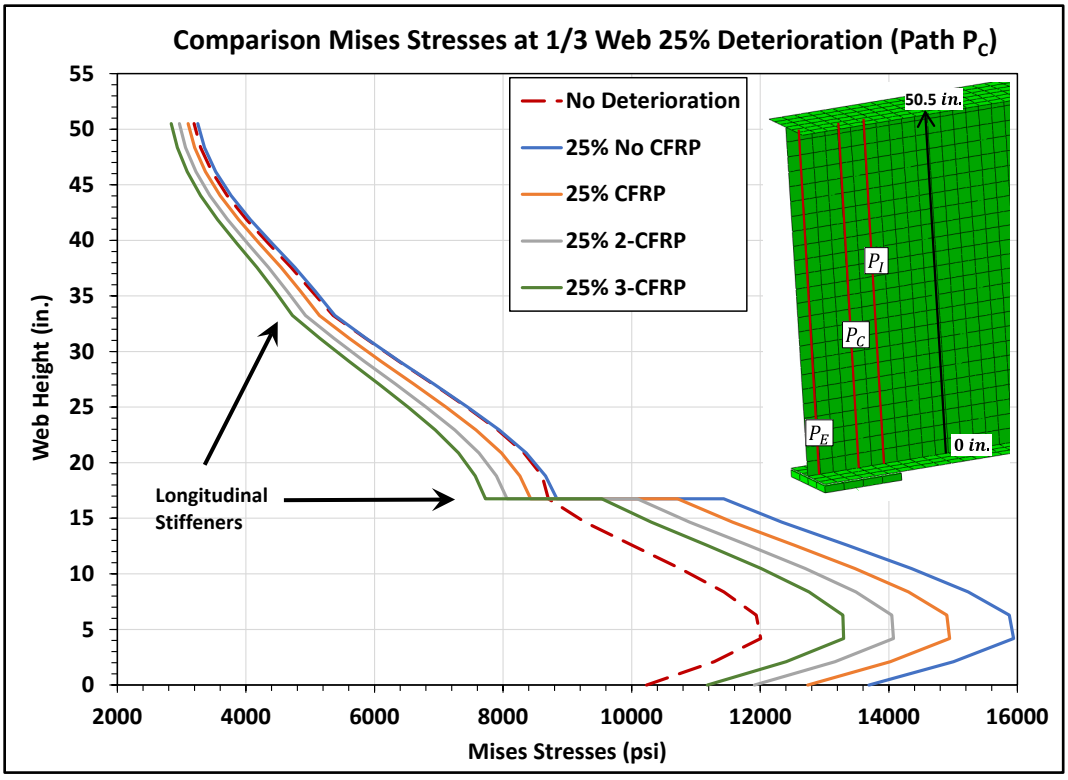

Figure 34. Comparison of the von Mises stresses produced along path P_I for the bottom one-third of the web with no deterioration and 25% deterioration with CFRP, 2-CFRP, and 3-CFRP.

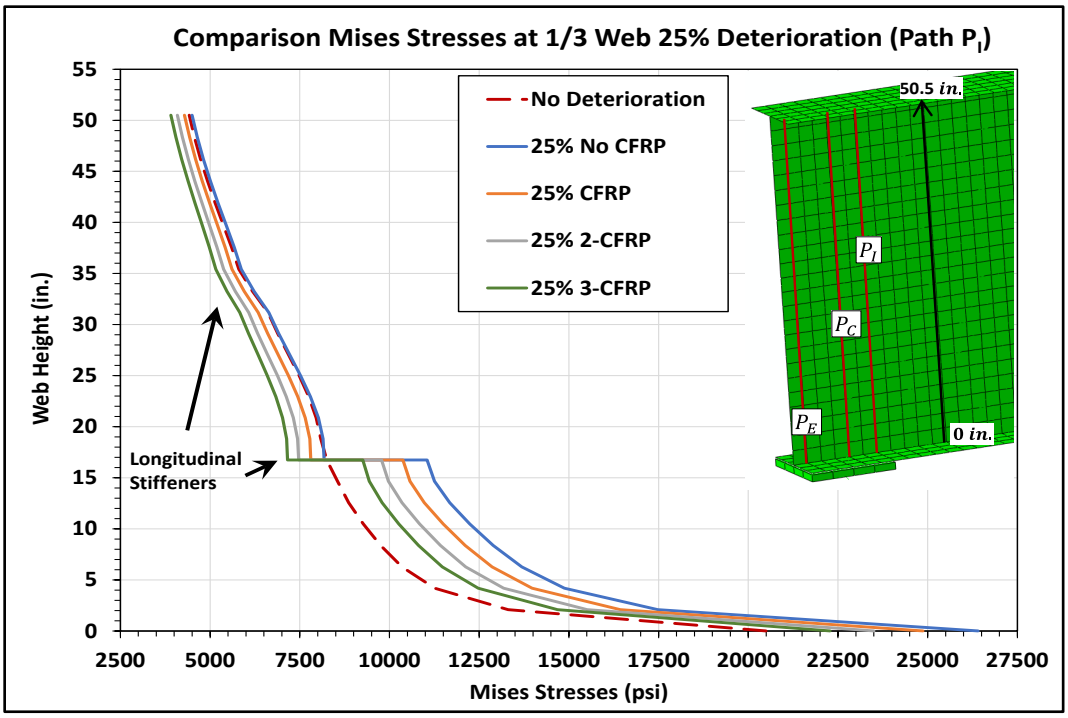

Figure 35. Comparison of the von Mises stresses produced along path P_E the bottom one-third of the web with no deterioration and the five laminate configurations repairing the 25% deteriorated web.

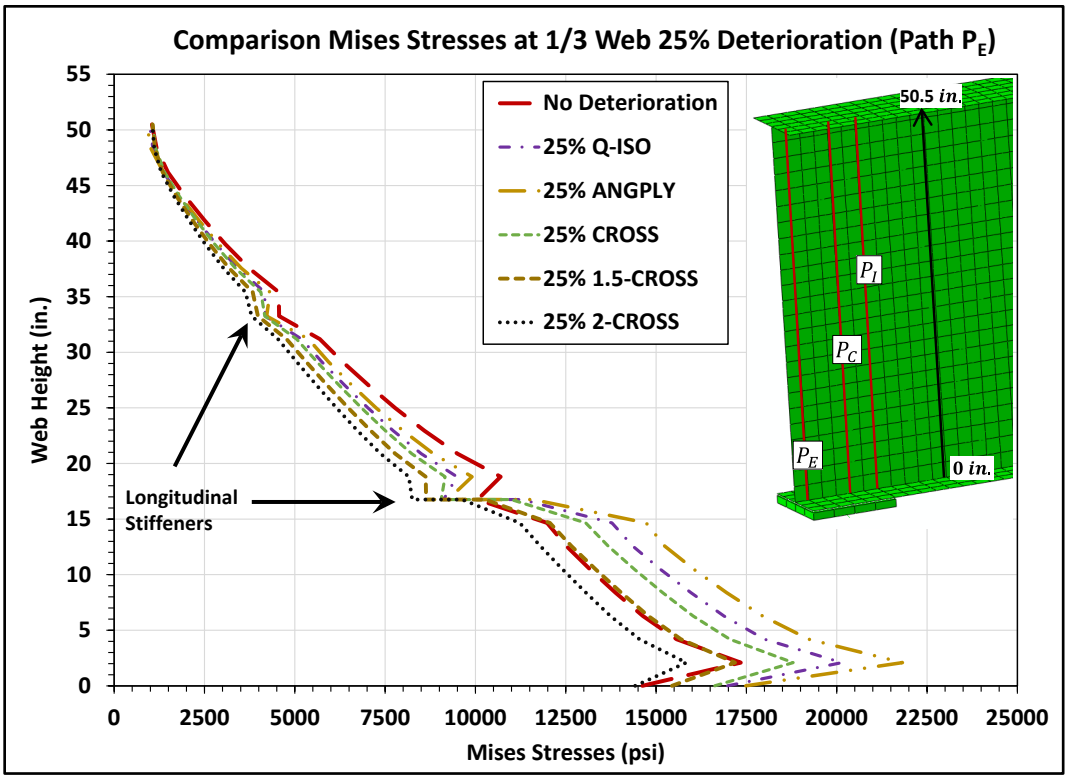

Figure 36. Comparison of the von Mises stresses produced along path P_C for the bottom one-third of the web with no deterioration and the five laminate configurations repairing the 25% deteriorated web.

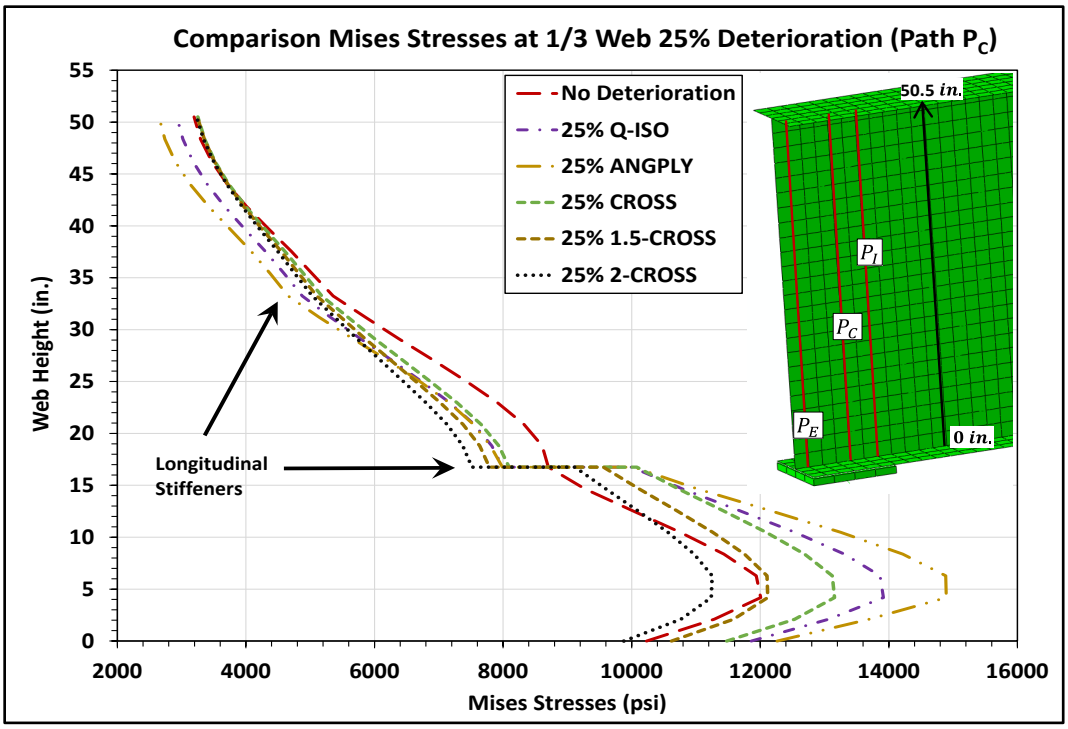

Figure 37. Comparison of the von Mises stresses produced along path P_I for the bottom one-third of the web with no deterioration and the five laminate configurations repairing the 25% deteriorated web.

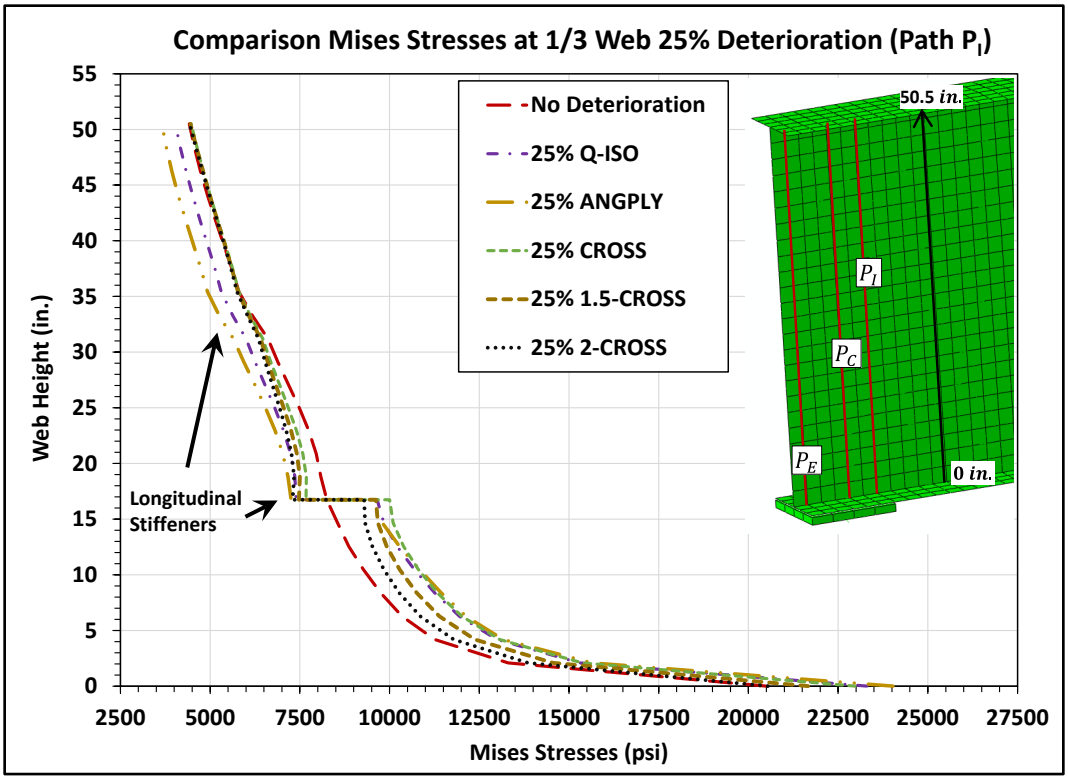

Figure 38. Comparison of the von Mises stresses produced along path P_E for the bottom two-thirds of the web with no deterioration and 25% deterioration with no CFRP, CFRP, 2-CFRP, and 3-CFRP.

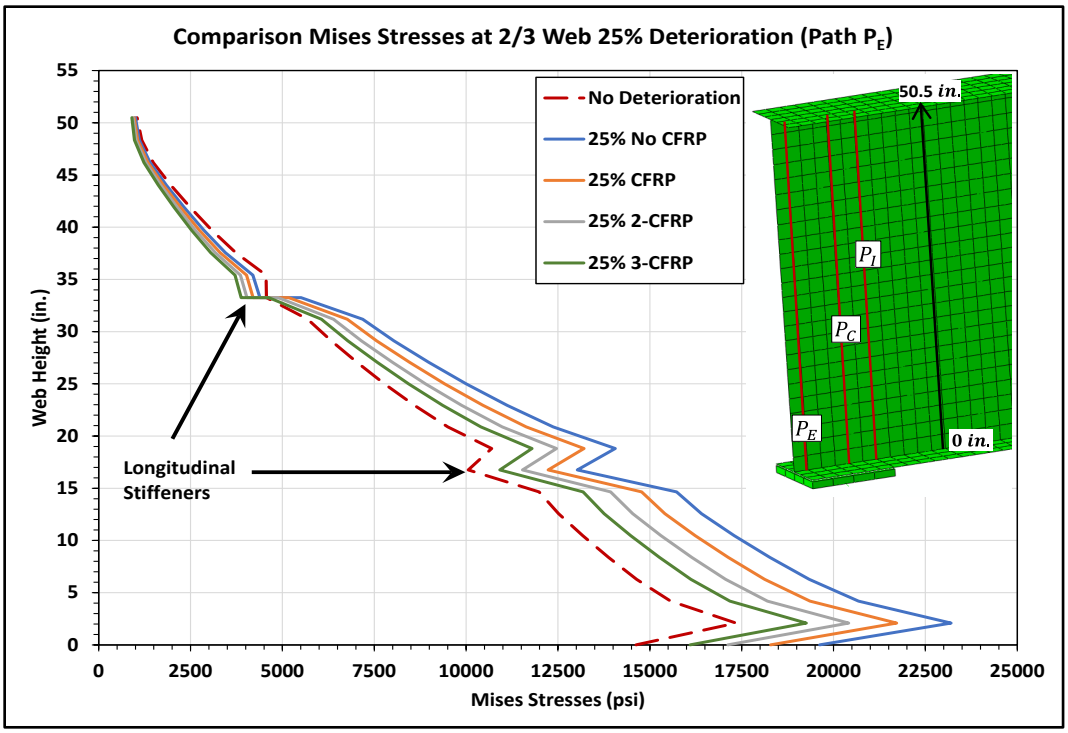

Figure 39. Comparison of the von Mises stresses produced along path P_C for the bottom two-thirds of the web with no deterioration and 25% deterioration with no CFRP, CFRP, 2-CFRP, and 3-CFRP.

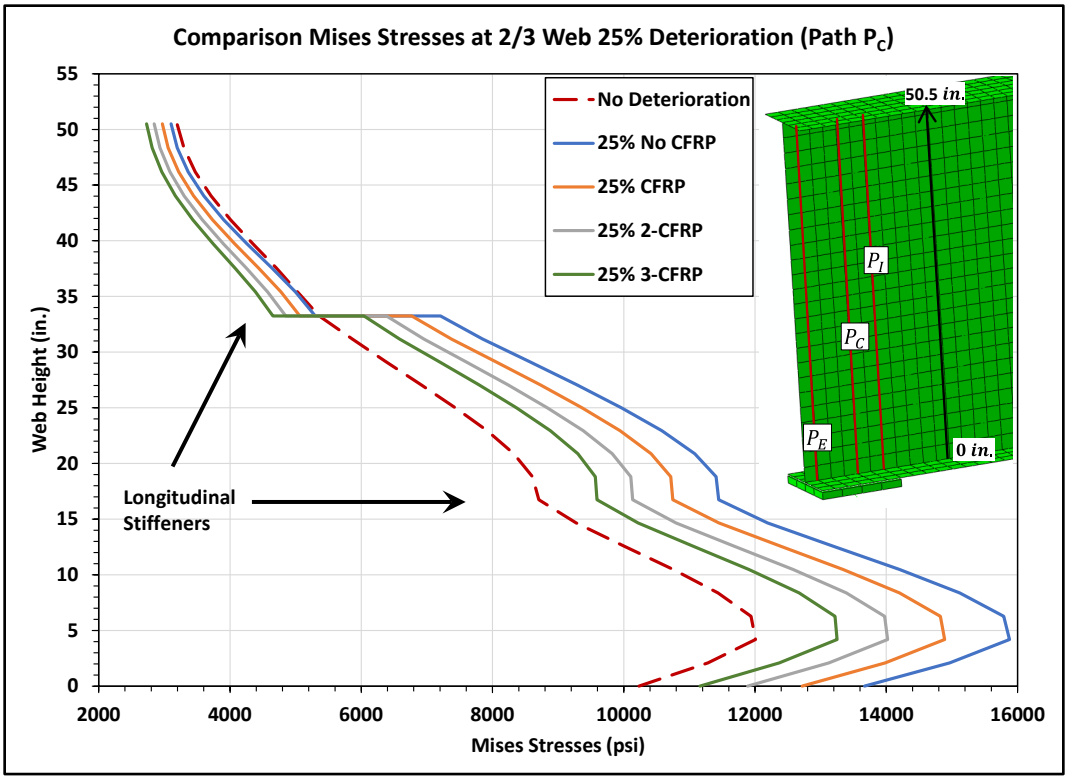

Figure 40. Comparison of the von Mises stresses produced along path P_I for the bottom two-thirds of the web with no deterioration and 25% deterioration with no CFRP, CFRP, 2-CFRP, and 3-CFRP.

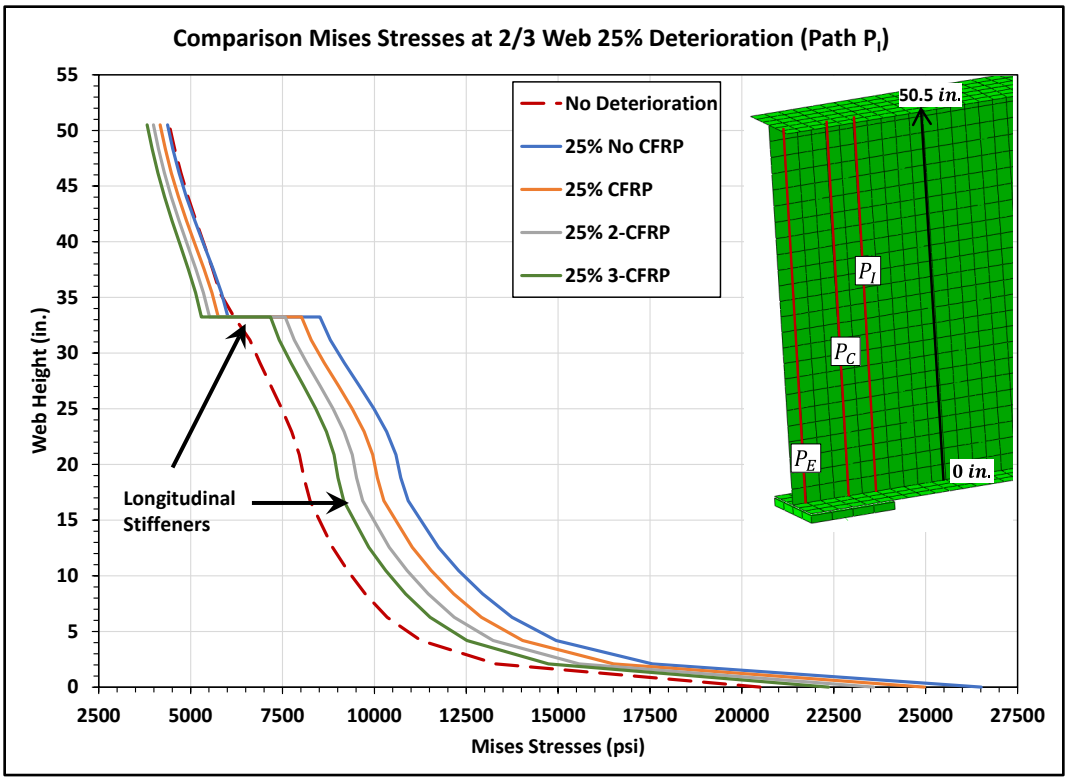

Figure 41. Comparison of the von Mises stresses produced along path P_E for the bottom two-thirds of the web with no deterioration and the five laminate configurations repairing the 25% deteriorated web.

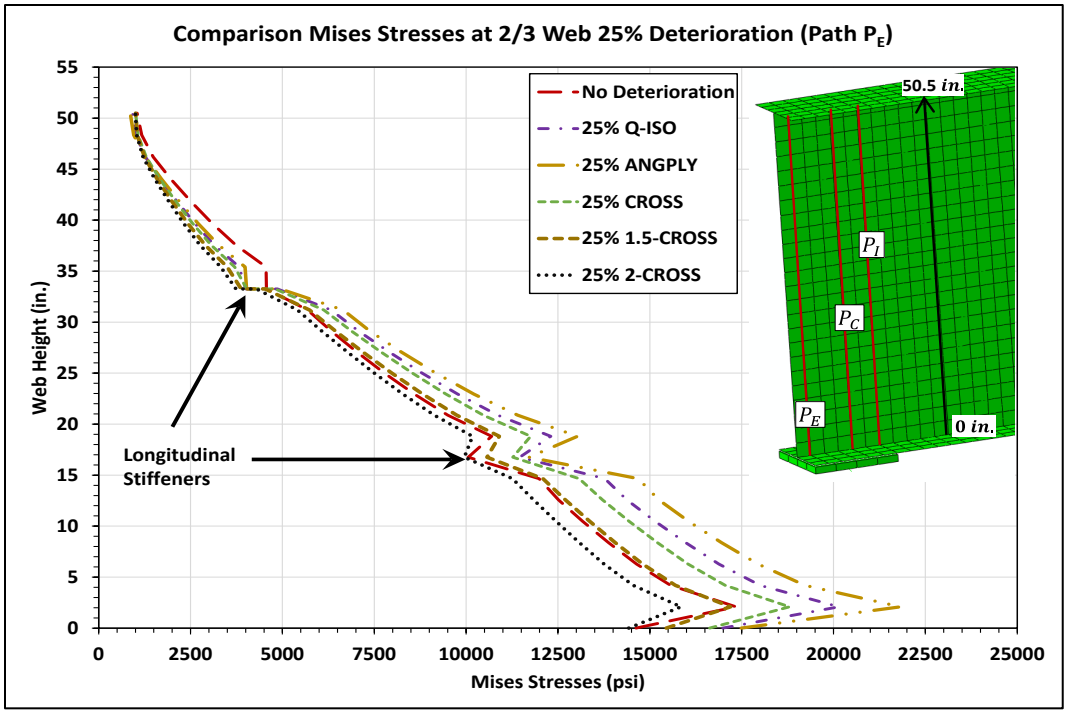

Figure 42. Comparison of the von Mises stresses produced along path P_C for the bottom two-thirds of the web with no deterioration and the five laminate configurations repairing the 25% deteriorated web.

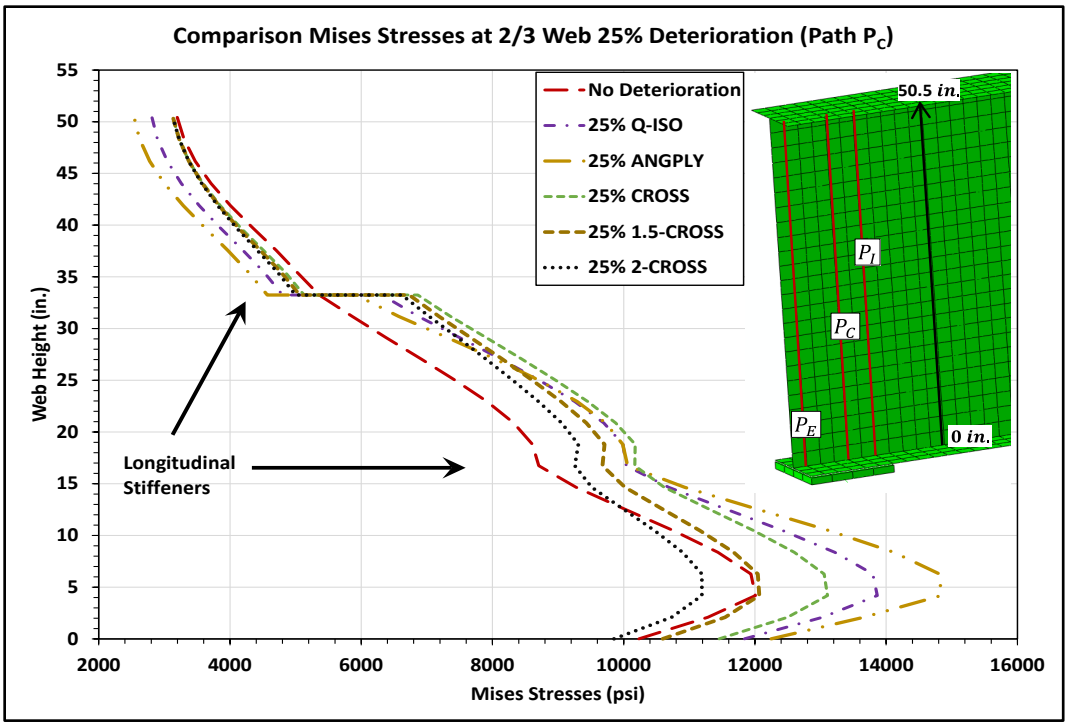

Figure 43. Comparison of the von Mises stresses produced along path P_I for the bottom two-thirds of the web with no deterioration and the five laminate configurations repairing the 25% deteriorated web.

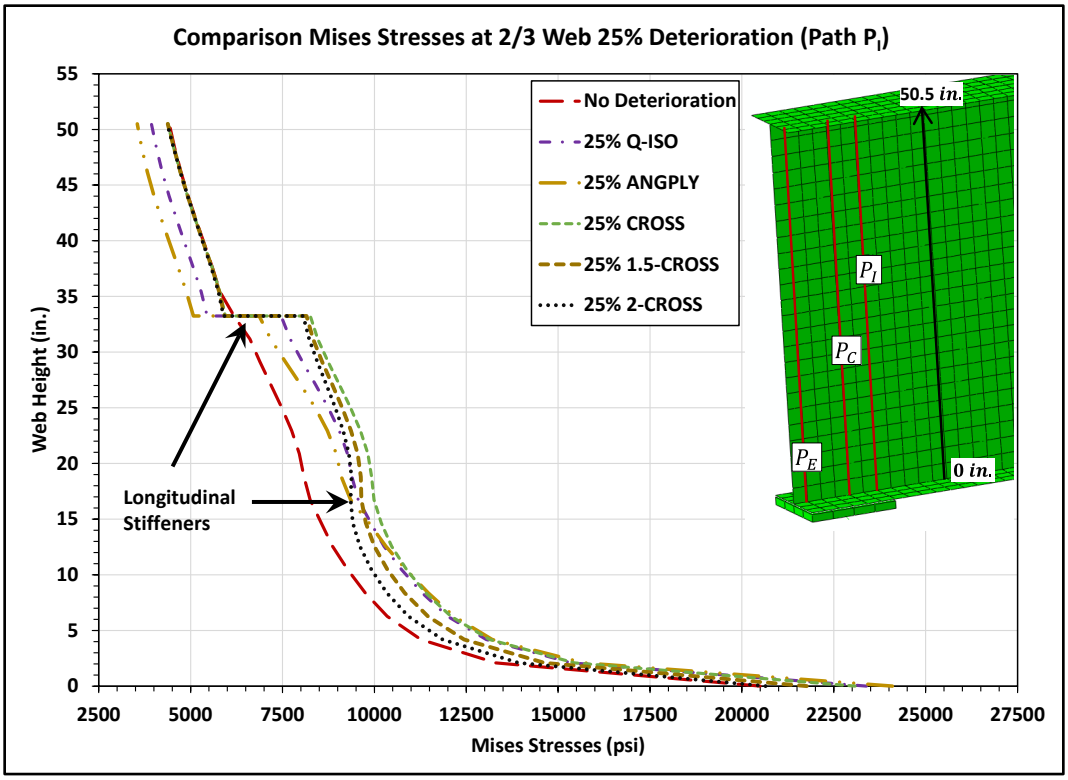

3.3.2 Bending (Tension) Dominated Zone

Because the principal stresses that dominate the bottom flange in tension of the beam run parallel to the longitudinal axis of the girder, the laminate used to repair a damaged flange will only run in the longitudinal direction. No layup schemes with fibers running in other directions are needed. In this case, only the number of unidirectional layers is reported.

Figure 44 shows the path location between the edge of the flange and the union with the web. Stresses S_{11} (from Abaqus) were extracted starting from midspan (symmetric plane) of the girder. The CFRP repair schemes were as explained in the previous section, and the length that it is covered is shown in the figure. The load at which the stresses were calculated was 131,640 lb higher than the load used for the shear zone.

Figure 44. Path used to extract longitudinal stresses (S_{11}) in the bottom flange of the girder.

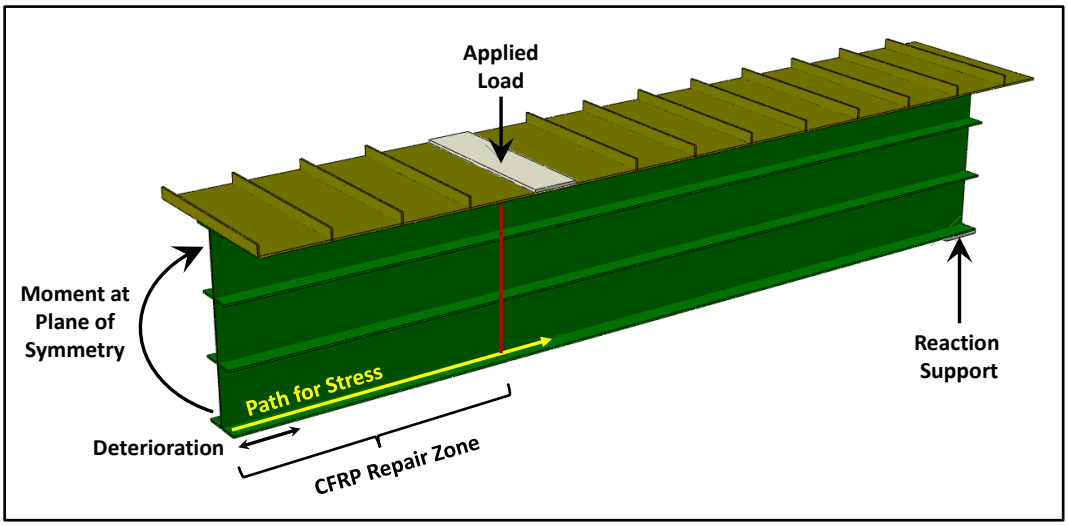

Figures 45–48 show results of the flange with 10% deterioration at lengths of 2, 4, and 8 times the flange width. From the analysis it is found that the stresses are reduced if only four layers of CFRP are used. It is also observed that the shorter deteriorated length (2×) produce higher stresses than the other three deterioration lengths.

All results show two stress concentration points as a localized increase and drop in the stress magnitudes. This is a numerically induced behavior from the radical transition of thicknesses between the deteriorated zone and the CFRP end location. In the actual application, the deteriorated zone is cleaned, and the rough edges are smoothed out. The CFRP layers can be

stopped in steps to create a smooth transition. It is interesting to see an increase in stresses immediately after the CFRP repair stops.

Figures 49–52 show results of the 25% tensile flange deterioration and CFRP repair. The CFRP applied pattern was from 1 to 4 layers, then 8 and 10 layers. Again, it can be observed that for the shorter deterioration length (2×), 10 layers of CFRP reduce the stresses in the steel to the point of the undamaged section. But as the length increases, 8 layers are sufficient to drop the stress levels to the undamaged condition. This is something that has to be accounted for when applying repair techniques.

As opposed to the shear (bearing) zone, the 40% deterioration level was also investigated applying the same repair techniques for the 25% case. These results are shown in Figures 53–56. It was found that for this level of deterioration, 10 layers of CFRP are not effective for the shorter deterioration lengths. Only for the larger deterioration zone (8×) is it observed that the effect of the repair is to reduce stresses to the undeteriorated magnitude. More layers of CFRP will be needed to repair such large deterioration and loss of section.

Figure 45. Comparison of tensile stresses with 10% deterioration along the bottom flange under repair scheme 2 times the flange width.

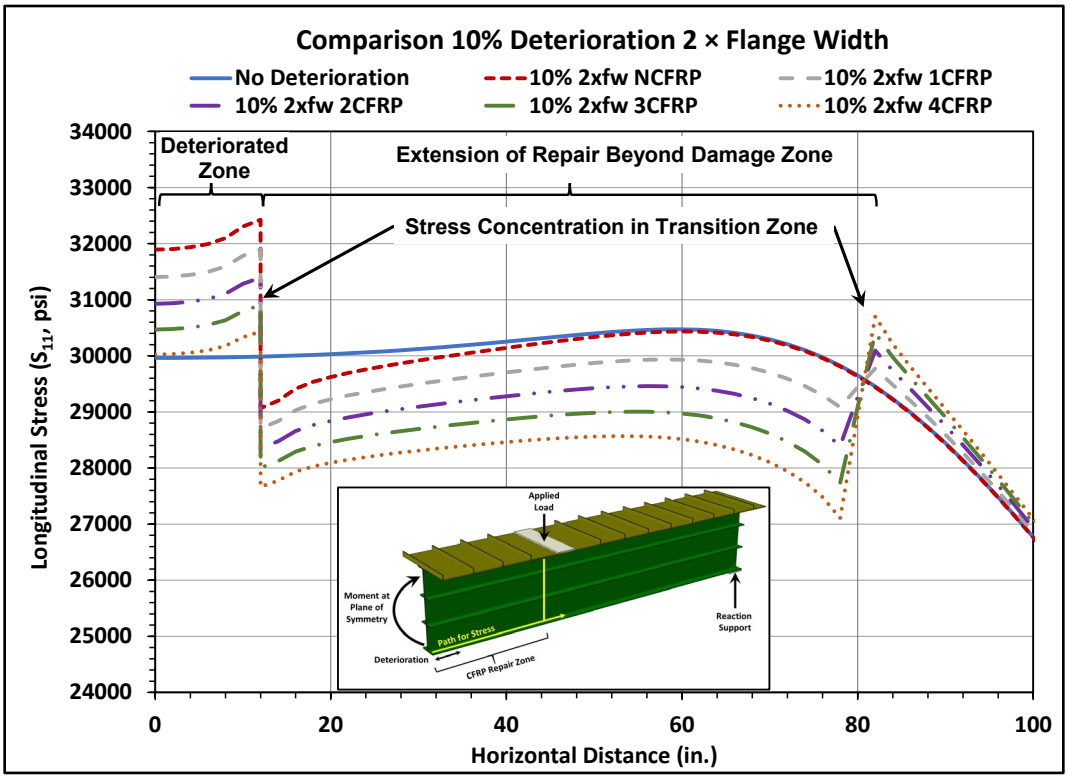

Figure 46. Comparison of tensile stresses with 10% deterioration along the bottom flange under repair scheme 4 times the flange width.

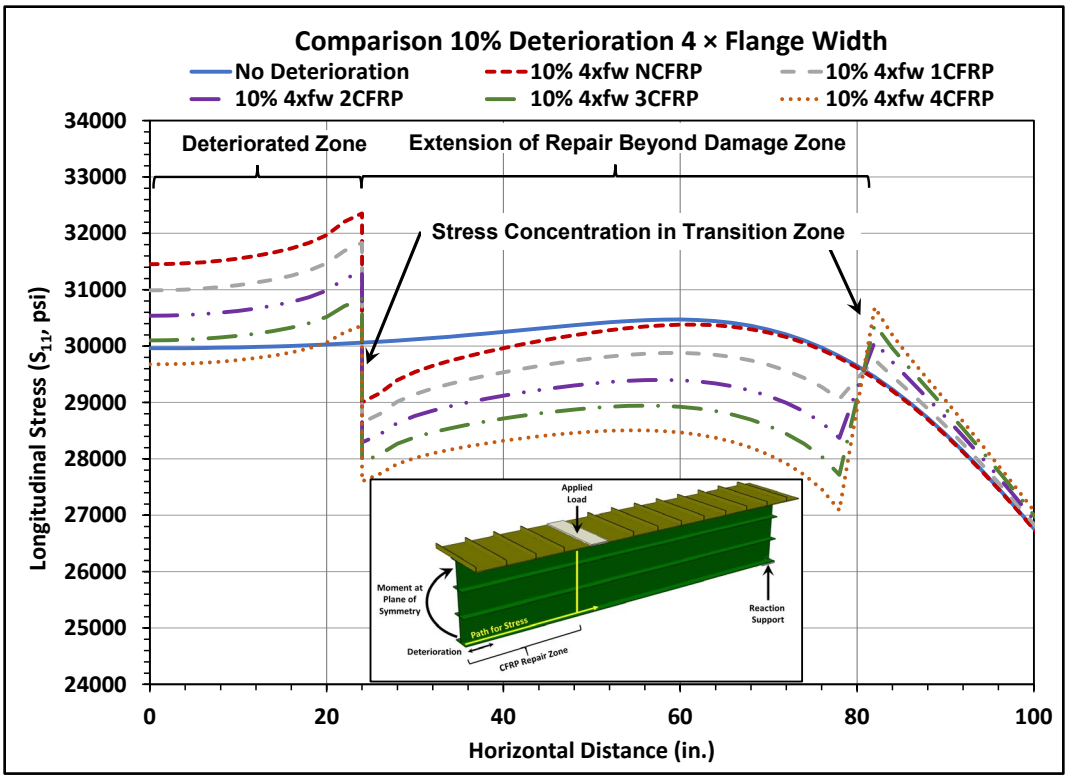

Figure 47. Comparison of tensile stresses with 10% deterioration along the bottom flange under repair scheme 6 times the flange width.

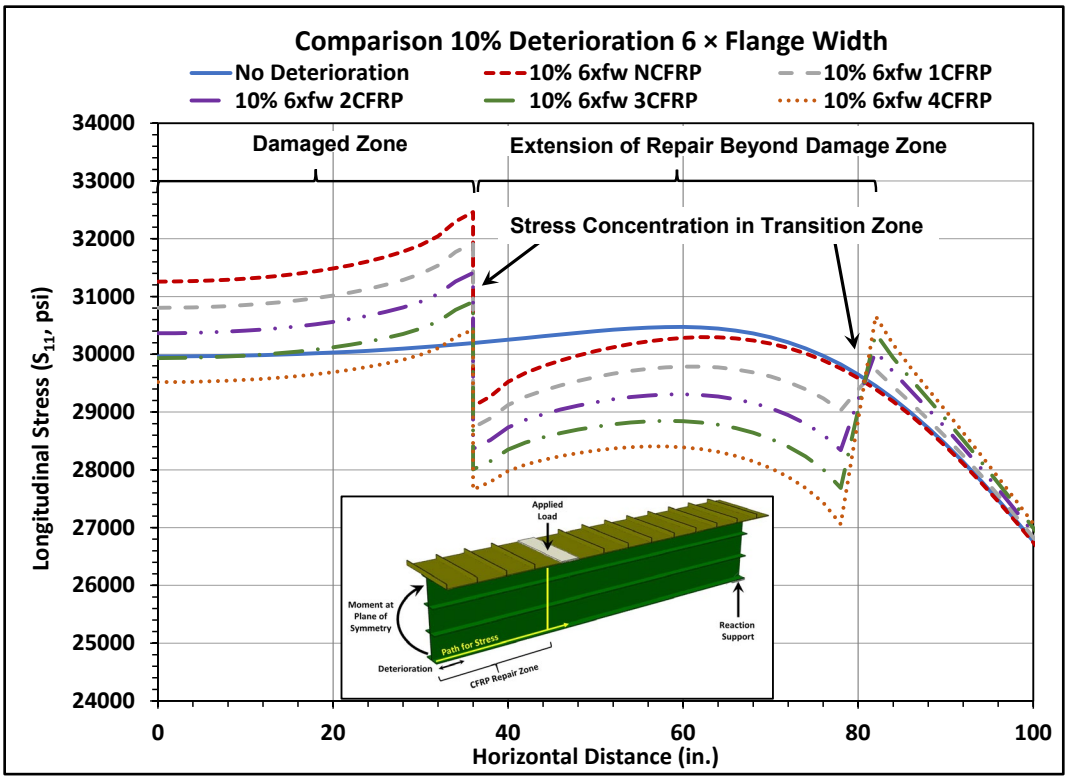

Figure 48. Comparison of tensile stresses with 10% deterioration along the bottom flange under repair scheme 8 times the flange width.

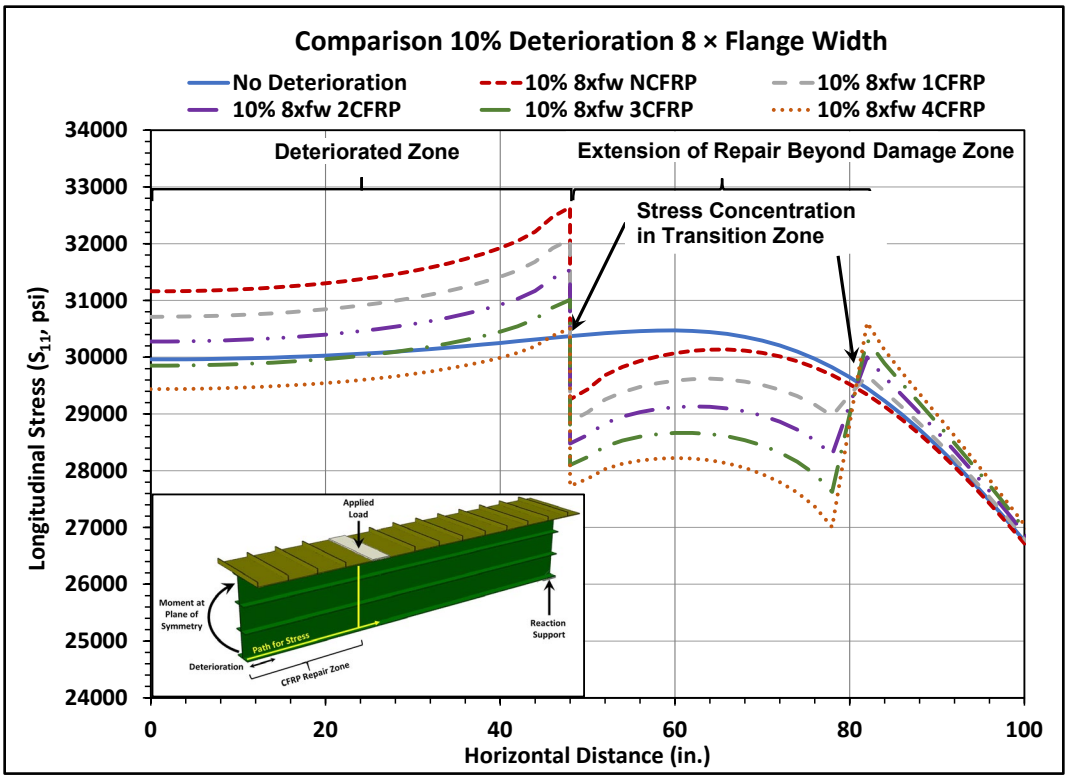

Figure 49. Comparison of tensile stresses with 25% deterioration along the bottom flange under repair scheme 2 times the flange width.

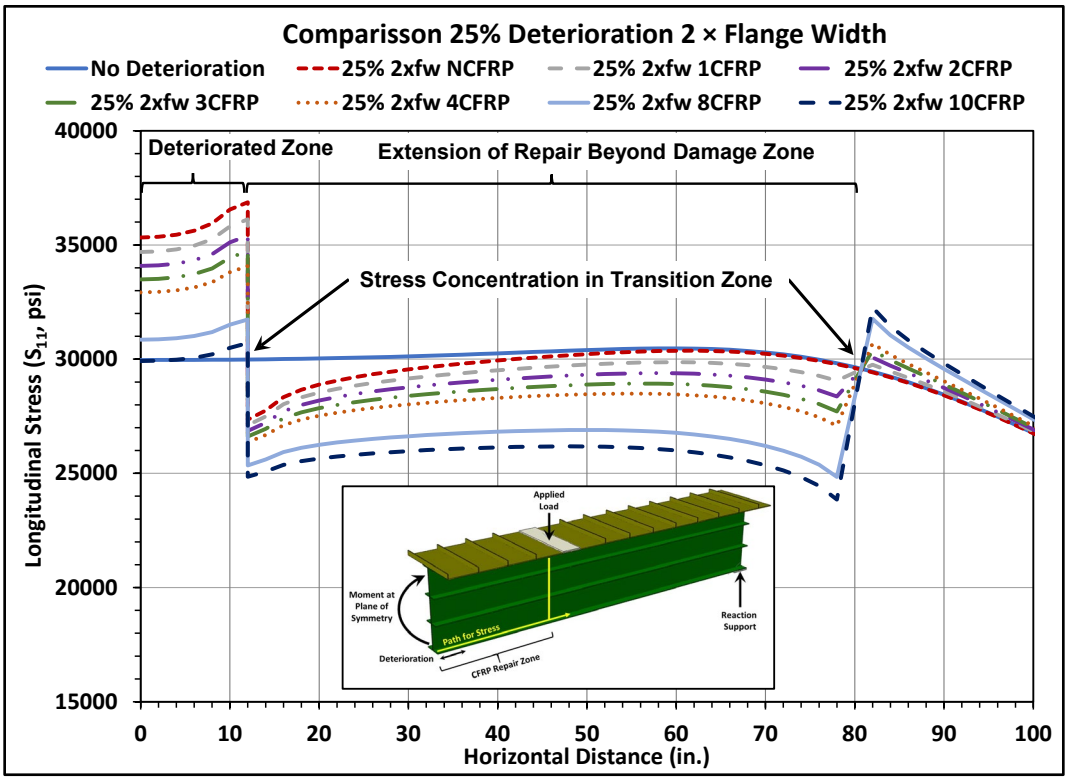

Figure 50. Comparison of tensile stresses with 25% deterioration along the bottom flange under repair scheme 4 times the flange width.

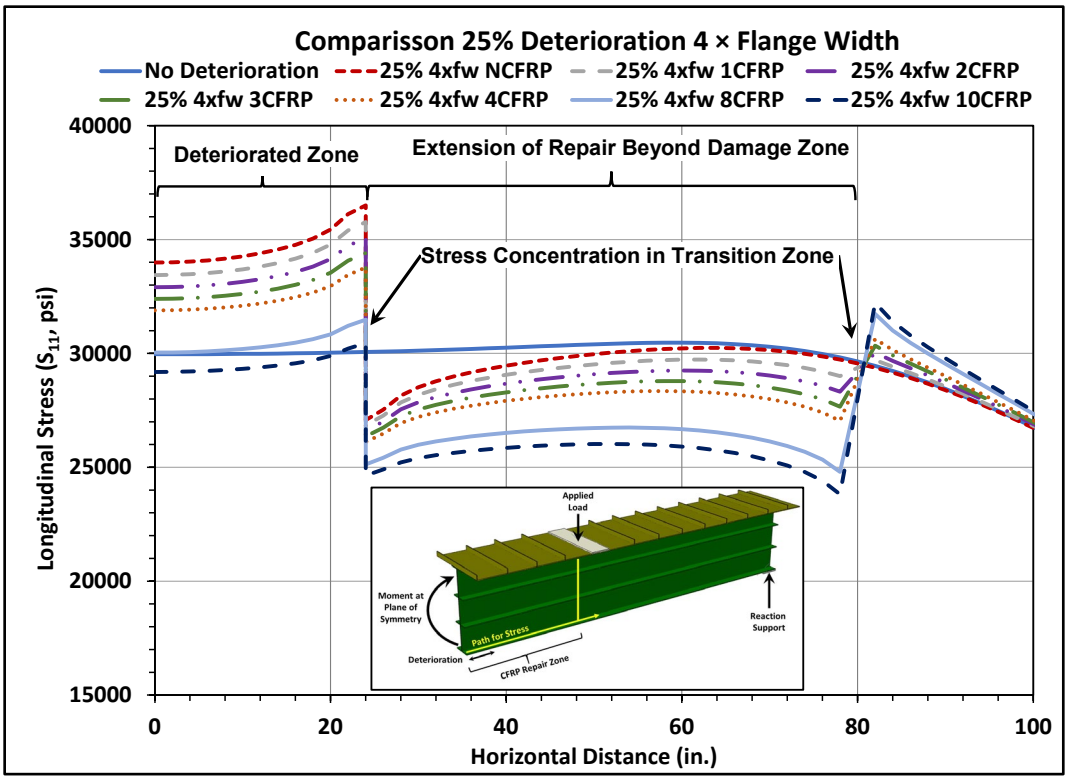

Figure 51. Comparison of tensile stresses with 25% deterioration along the bottom flange under repair scheme 6 times the flange width.

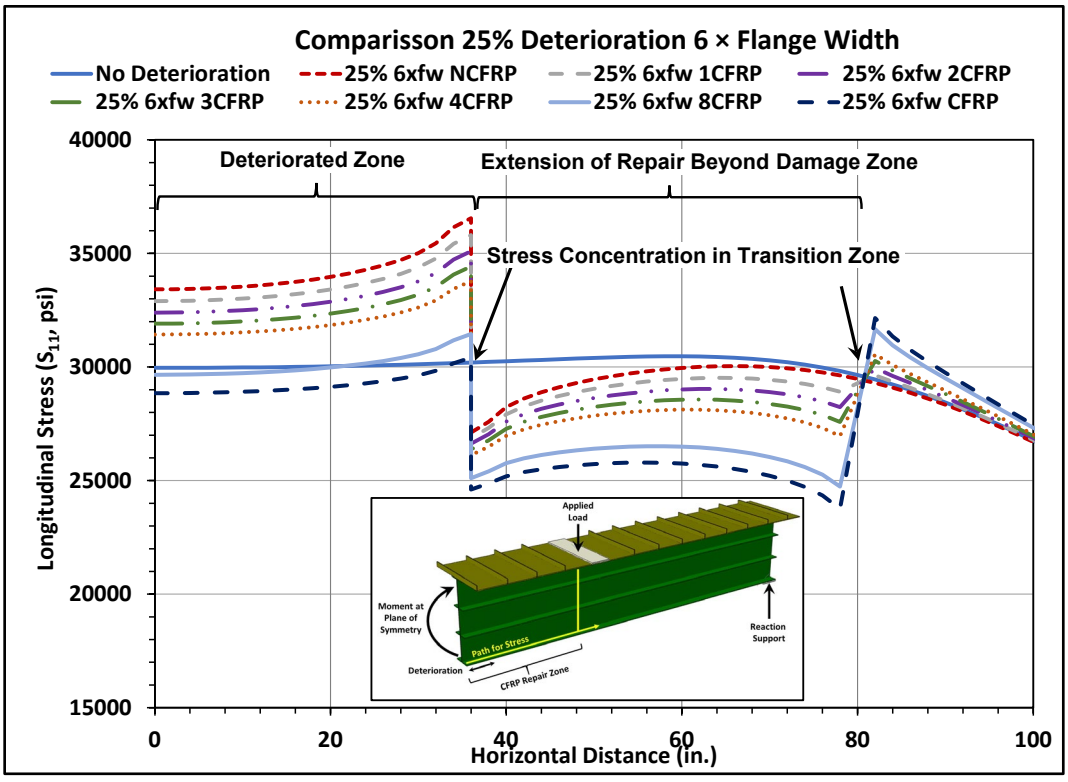

Figure 52. Comparison of tensile stresses with 25% deterioration along the bottom flange under repair scheme 8 times the flange width.

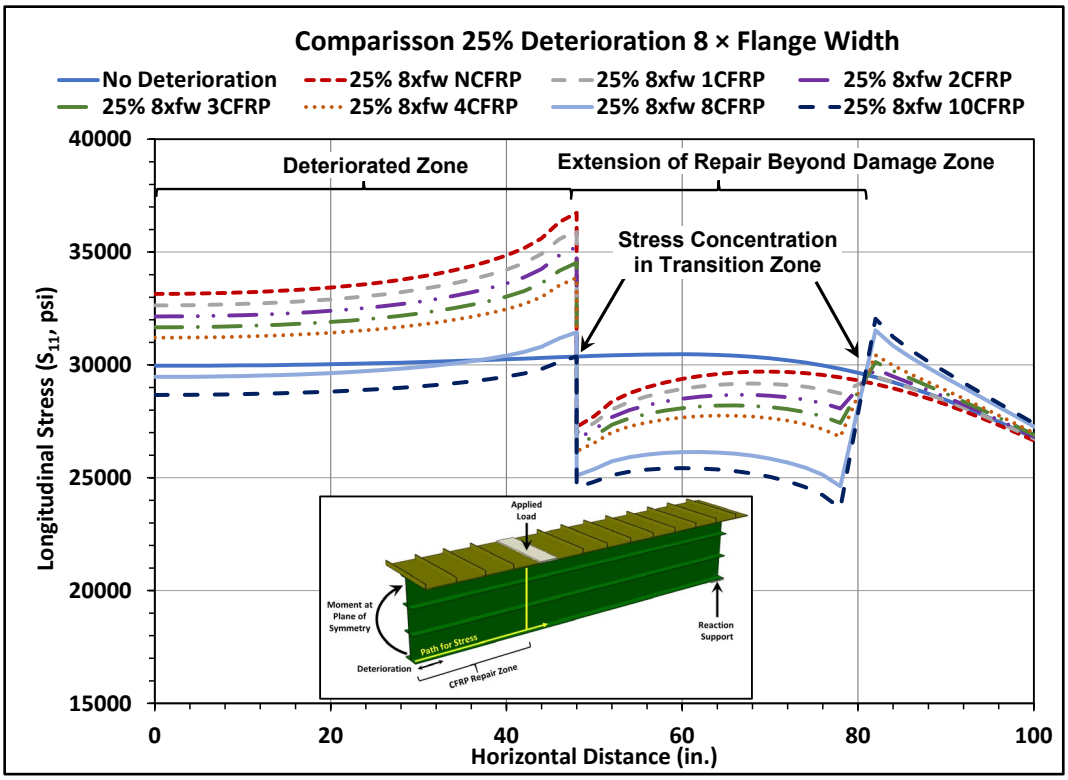

Figure 53. Comparison of tensile stresses with 40% deterioration along the bottom flange under repair scheme 2 times the flange width.

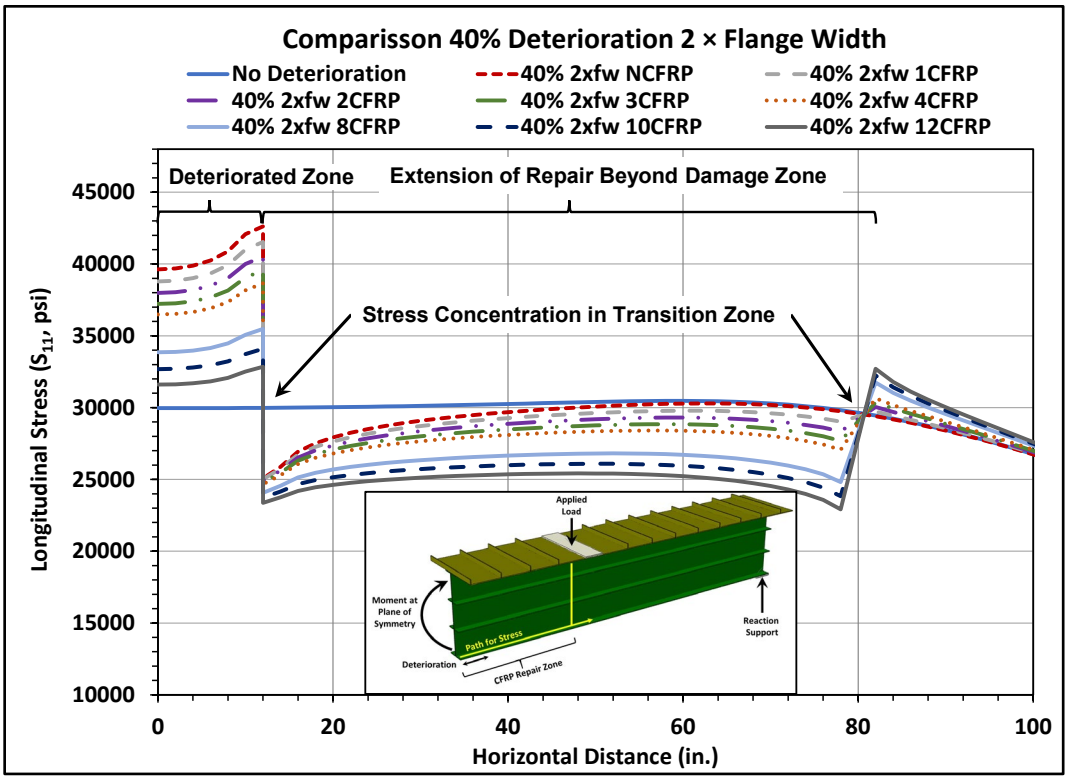

Figure 54. Comparison of tensile stresses with 40% deterioration along the bottom flange under repair scheme 4 times the flange width.

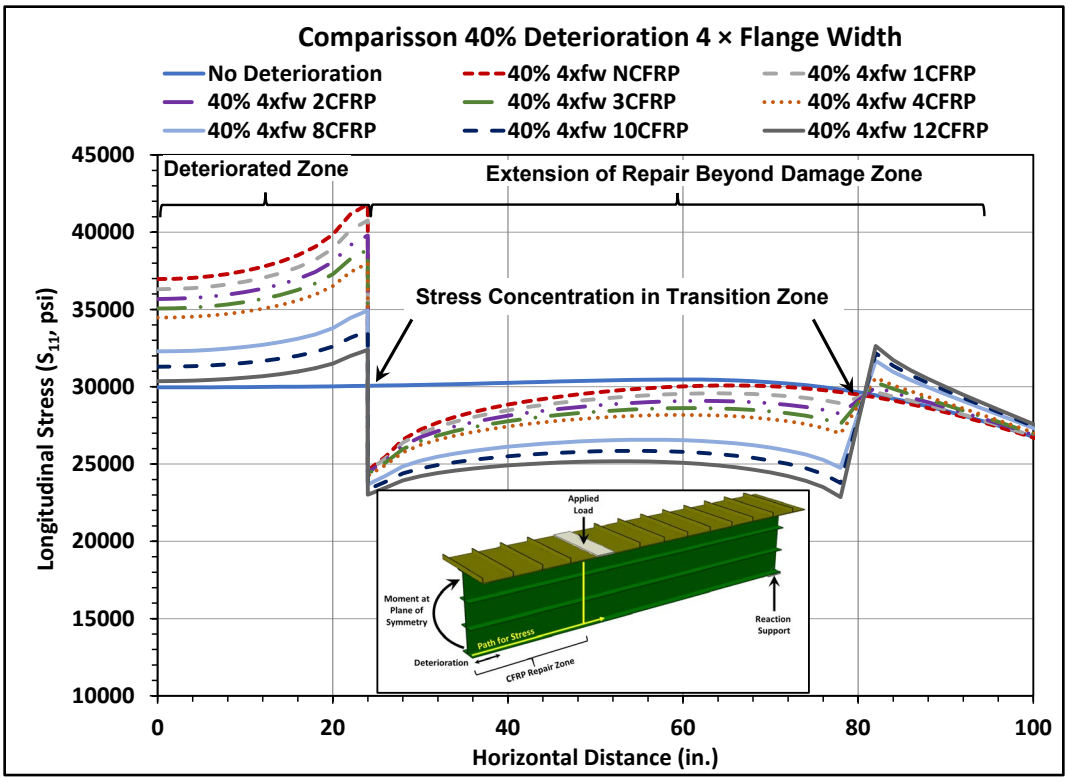

Figure 55. Comparison of tensile stresses with 40% deterioration along the bottom flange under repair scheme 6 times the flange width.

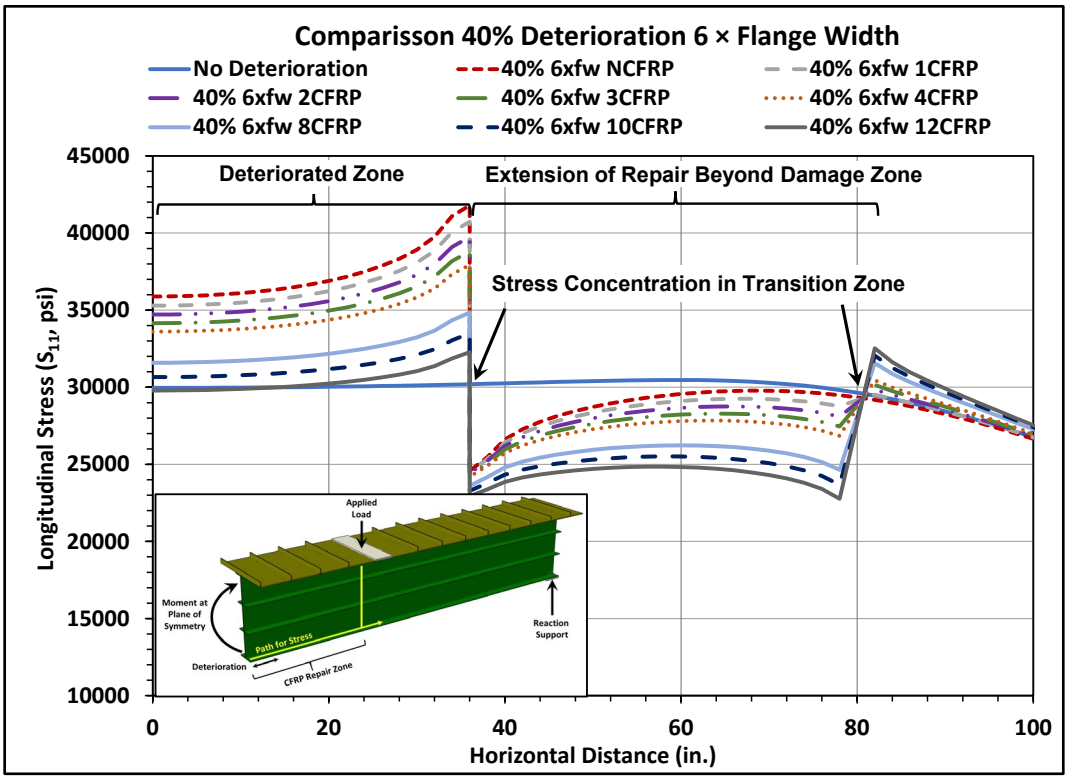

Figure 56. Comparison of tensile stresses with 40% deterioration along the bottom flange under repair scheme 2 times the flange width.

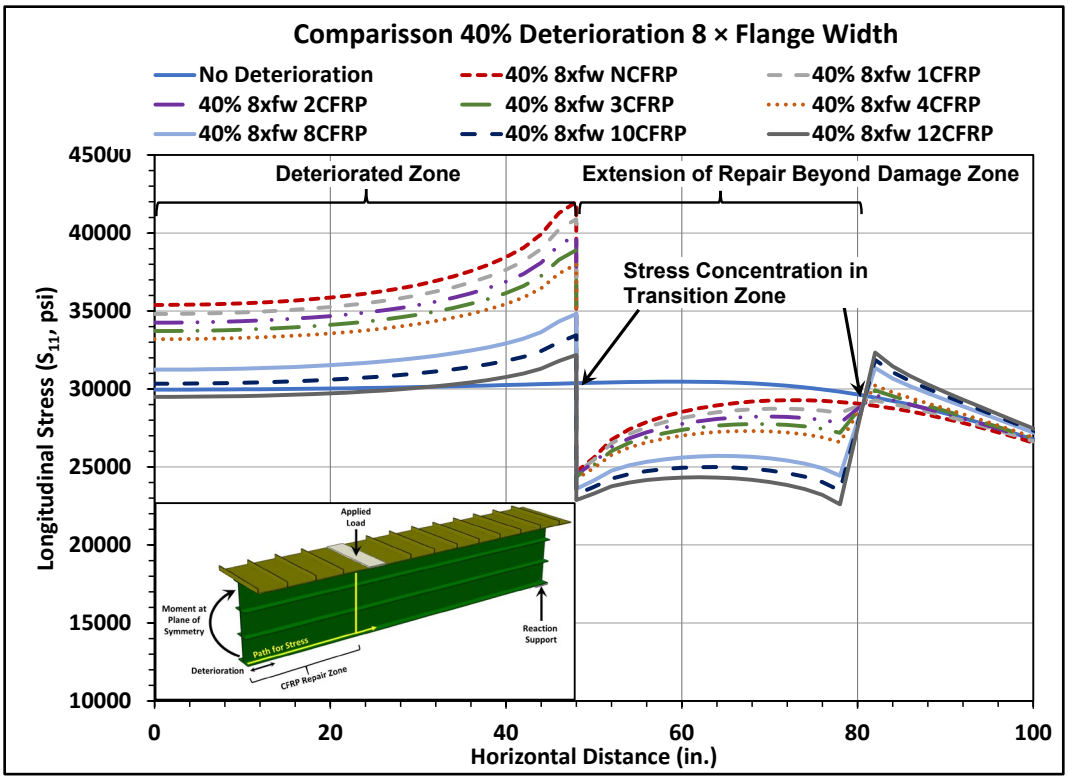

4 Conclusions

This report presents a study of the effect on the stress levels of corrosion deterioration of steel girders used in hydraulic structures. Additionally, the report presents the evaluation of the changes in stresses once the deteriorated girders are retrofitted with carbon fiber–reinforced polymers (CFRP). These girders are heavily constrained in the gates by nearby elements such as the skin plate, transverse beams, and the end elements, quoin pin end and miter end. However, the boundary conditions and loading patterns used were simplified to simply supported with four-point loading. The corrosion deterioration was modeled as loss in section at 10%, 25%, 40%, and 50% levels. For the shear (bearing) zone, only 10% and 25% were evaluated because preliminary results showed that CFRP will not be practical and effective for section losses beyond 25%. However, for the tensile dominated zone, at the bottom flange at midspan, 10%, 25%, and 40% deterioration were evaluated. The level of load applied to each model was below the load required to trigger yielding at the tensile flange. The effectiveness of the deterioration was established based on the level of stresses at the steel compared with the undamaged condition after it is strengthened with CFRP.

In this work, it was found that the equivalent isotropic material properties (CFRP) layouts do not provide sufficient strength recovery compared to using the laminate layouts. For the shear dominated zone at 10% deterioration, the CFRP layout angle-ply is not as effective as the other proposed laminate layups. At 25% deterioration, the proposed schemes are not effective for lowering the stresses at the deteriorated steel: more layers are needed to repair higher levels of deterioration.

This indicates that the CFRP thickness of one layer needs to be increased to obtain a better performance of the repairs.

The tensile dominated zone at midspan bottom flange can be repaired using only unidirectional fibers oriented in the longitudinal direction of the girder. For the 10% deterioration level, up to 4 layers of CFRP are sufficient to reduce the stresses at the steel. For 25% deterioration, at least 10 layers of CFRP can reduce the stresses in the steel to satisfactory levels. If the level of deterioration is 40%, 10 layers of CFRP are effective when the extension of the deterioration is 8 times flange width.

Furthermore, the analysis showed stress concentrations are generated at the transition zones of deterioration. This behavior is produced by the numerical model that has an abrupt change in cross-section stiffness. Also, stress concentrations are generated at the point of termination of the CFRP repair, also produced by the abrupt change in cross-section. Therefore, it is recommended that spew fillets at the end of the patches with additional adhesive be implemented to create a smooth transition.

Bibliography

AISC (American Institute of Steel Construction). 2017. *Steel Construction Manual*, 15th ed. Chicago: American Institute of Steel Construction.

Andresen, H. W., and A. T. Echtermeyer. 2006. "Critical Energy Release Rate for a CSM Reinforced Carbon Fibre Composite/Steel Bonding." *Composites Part A: Applied Science and Manufacturing* 37 (5): 742–51. https://doi.org/10.1016/j.compositesa.2005.06.009.

Barbero, E. J. 2010. *Introduction to Composite Materials Design*, 2nd ed. London: Taylor and Francis.

Da Costa Mattos, H. S., J. M. L. Reis, L. M. Paim, M. L. Da Silva, F. C. Amorim, and V. A. Perrut. 2014. "Analysis of a Glass Fibre Reinforced Polyurethane Composite Repair System for Corroded Pipelines at Elevated Temperatures." *Composite Structures* 114 (1): 117–23. https://doi.org/10.1016/j.compstruct.2014.04.015.

Dassault Systèmes. 2015. *Abaqus/CAE User's Guide*. Waltham, MA.

Dexter, R., H. N. Mahmoud, J. A. Padula, and G. Riveros. 2007. *Fitness for Purpose Evaluation of Hydraulic Steel Structures*. ERDC TR-07-15. Vicksburg, MS: US Army Corps of Engineers Research and Development Center. https://erdclibrary.erdc.dren.mil/jspui/handle/11681/8510.

Gibson, R. F. 2016. *Principles of Composite Material Mechanics*, 4th ed. Boca Raton, FL: CRC Press.

Haghani, R., and M. Al-Emrani. 2012. "A New Design Model for Adhesive Joints Used to Bond FRP Laminates to Steel Beams Part B: Experimental Verification." *Construction and Building Materials* 30: 686–94. https://doi.org/10.1016/j.conbuildmat.2011.12.005.

Jayasuriya, S., A. Bastani, S. Kenno, T. Bolisetti, and S. Das. 2018. "Rehabilitation of Corroded Steel Beams Using BFRP Fabric." *Structures* 15 (March): 152–61. https://doi.org/10.1016/j.istruc.2018.06.006.

Kayser, J. R., and A. S. Nowak. 1989. "Capacity Loss Due to Corrosion in Steel-Girder Bridges." *Journal of Structural Engineering* 115 (6): 1525–37.

Mahmoud, H., M. Memari, and B. Atadero. 2018 "Experimental Fatigue Assessment of CFRP-Retrofitted RC Bridge Beams Subjected to High Service Temperatures." *Published Date : 2018-08-01. Report Number: MPC-18-362.* https://rosap.ntl.bts.gov/view/dot/44228.

Mitra, S., A. Bastani, S. Das, and D. Lawn. 2020. "Corroded Steel Beams with Various Corrosion Aspect Ratios—A Rehabilitation Technique Using Basalt Fibre Fabric. *Engineering Structures* 221 (June): 111075. https://doi.org/10.1016/j.engstruct.2020.111075.

Mitra, S., A. Bastani, S. Das, and D. Lawn. 2022. "Corroded Steel Beams with Various Corrosion Aspect Ratios—A Rehabilitation Technique Using Basalt Fibre Fabric." *Engineering Structures* 221: 1–12.

Riveros, G., and E. Arredondo. 2010. *Predicting Deterioration of Navigation Steel Hydraulic Structures with Markov Chain and Latin Hypercube Simulation*. ERDC/CHL CHETN-IX-24. Vicksburg, MS: Engineer Research Development Center. https://hdl.handle.net/11681/2054.

Riveros, G. A., F. J. Acosta, C. M. Lozano, and E. Glynn. 2022. "The Effects of Deteriorated Boundary Conditions on Horizontally Framed Miter Gates." *Metals* 12: 37. https://doi.org/10.3390/met12010037.

Riveros, G. A., and E. Arredondo. 2014. "Predicting Future Deterioration of Hydraulic Steel Structures with Markov Chain and Multivariate Samples of Statistical Distributions." *Journal of Applied Mathematics* 2014: 360532–360532.

Riveros, G., H. Mahmoud, and C. Lozano. 2018. "Fatigue Repair of Underwater Navigation Steel Structures Using Carbon Fiber Reinforced Polymer (CFRP)." *Engineering Structures* 173: 718–28, https://doi.org/10.1016/j.engstruct.2018.07.016.

Sauser, P. W., and G. A. Riveros. 2009. *A System for Collecting and Compiling Condition Data for Hydraulic Steel Structures for Use in the Assessment of Risk and Reliability and Prioritization of Maintenance and Repairs*. ERDC/ITL TR-09-04. Vicksburg, MS: Engineer Research and Development Center. https://hdl.handle.net/11681/10950.

Sirimanna, C. S., S. Banerjee, W. Karunasena, A. C. Manalo, and L. McGarva. 2015. "Analysis of Retrofitted Corroded Steel Pipes Using Internally Bonded FRP Composite Repair Systems." *Australian Journal of Structural Engineering* 16 (3): 187–98. https://doi.org/10.1080/13287982.2015.1092681.

Abbreviations

BFRP	Basalt fiber–reinforced polymer
CFRP	Carbon fiber–reinforced polymer
FRP	Fiber-reinforced polymer
Fw	Flange width
HSS	Hydraulic steel structure
ROM	Rules of mixtures

REPORT DOCUMENTATION PAGE

1. REPORT DATE	2. REPORT TYPE	3. DATES COVERED	
		START DATE	END DATE
August 2023	Final technical report	FY18	FY21

4. TITLE AND SUBTITLE

Repair of Corroded Steel Girders of Hydraulic Steel Structures (HSS) Using Fiber-Reinforced Polymers (FRP)

5a. CONTRACT NUMBER	5b. GRANT NUMBER	5c. PROGRAM ELEMENT
5d. PROJECT NUMBER	**5e. TASK NUMBER**	**5f. WORK UNIT NUMBER**

6. AUTHOR(S)

Felipe J. Acosta and Guillermo A. Riveros

7. PERFORMING ORGANIZATION NAME(S) AND ADDRESS(ES)

US Army Engineer Research and Development Center
Information Technology Laboratory
3909 Halls Ferry Road
Vicksburg, MS 39180-6199

8. PERFORMING ORGANIZATION REPORT NUMBER

ERDC/ITL TR-23-3

9. SPONSORING/MONITORING AGENCY NAME(S) AND ADDRESS(ES)

Engineer Research Development Center
Navigation Systems Research Program
Vicksburg, MS 39180-6199

10. SPONSOR/MONITOR'S ACRONYM(S)

NSRP

11. SPONSOR/MONITOR'S REPORT NUMBER(S)

12. DISTRIBUTION/AVAILABILITY STATEMENT

DISTRIBUTION STATEMENT A. Approved for public release; distribution is unlimited.

13. SUPPLEMENTARY NOTES

Work Unit 05D8DB, "FRP to strengthen deteriorated HSS," Funding Account Code U4388303 / AMSCO Code 031391

14. ABSTRACT

Although steel hydraulic structures have a protective system to prevent corrosion, this type of deterioration will eventually occur due to the constant exposure to harsh environmental conditions. There are several techniques that can be implemented to repair corroded steel structural elements. This report presents a numerical study to evaluate the mechanical behavior of corroded steel girders used in hydraulic steel structures and to evaluate several carbon fiber–reinforced polymers (CFRP) layups to repair them. The girders were modeled as simply supported with four-point loading boundary conditions. The corrosion deterioration was modeled as loss in section as 10%, 25%, and 40%. The effectiveness of the deterioration was established based on the level of stresses at the steel compared with the undamaged condition after it is strengthened with CFRP. It was found that CFRP repair is more practical for reducing the stresses at the steel in the shear dominated zone if deterioration is below 25%. At the tensile dominated zone, CFRP is effective for reducing the stresses for deterioration below 40%.

15. SUBJECT TERMS

Carbon fiber-reinforced plastics; Hydraulic structures--Maintenance and repair; Steel, Structural--Corrosion; Steel, Structural--Maintenance and repair

16. SECURITY CLASSIFICATION OF:			17. LIMITATION OF ABSTRACT	18. NUMBER OF PAGES
a. REPORT	b. ABSTRACT	C. THIS PAGE		
Unclassified	Unclassified	Unclassified	SAR	61

19a. NAME OF RESPONSIBLE PERSON	19b. TELEPHONE NUMBER (include area code)